Study of *CP* violation in hyperon decays at super-charm-tau factories with a polarized electron beam

Nora Salone,[1] Patrik Adlarson,[2] Varvara Batozskaya,[3,1] Andrzej Kupsc,[2,1,*] Stefan Leupold,[2] and Jusak Tandean[4]

[1]*National Centre for Nuclear Research, Pasteura 7, 02-093 Warsaw, Poland*
[2]*Department of Physics and Astronomy, Uppsala University, Box 516, SE-75120 Uppsala, Sweden*
[3]*Institute of High Energy Physics, Beijing 100049, People's Republic of China*
[4]*Surabaya, Gayungsari III/20, Surabaya 60235, Indonesia*

(Received 21 April 2022; accepted 10 June 2022; published 27 June 2022)

Nonleptonic two-body weak decays of baryons are an important tool to probe the combined charge conjugation–parity symmetry (*CP*) violation. We explain why the decays of strange baryons provide complementary information to the decays of kaons. A model-independent parametrization of the nonleptonic decays of the Λ and Ξ baryons is reviewed, and the amplitudes are updated according to the latest experimental input. We demonstrate the potential of performing precision tests in strange baryon decays at the next-generation electron-positron J/ψ factories with luminosity of 10^{35} cm^{-2} s^{-1}. The copious production of spin-entangled hyperon-antihyperon pairs via the J/ψ resonance allows for a direct comparison of the baryon and antibaryon decay properties. Using analytic approximations and numerical calculations, we study the quantitative impact of spin correlations and polarization in such *CP* tests. We show that by using a longitudinally polarized electron beam the statistical precision of the *CP* tests can be significantly improved compared to the experiments without polarized beams. Furthermore, we map out further directions for possible improvements, like analysis of incompletely reconstructed events or a combination of the isospin related processes. Altogether, these methods are promising for the observation of a statistically significant *CP*-violation signal with a strength corresponding to the standard model predictions. Our conclusions should encourage more detailed feasibility studies, including optimization of the measurement methods and studies of systematic effects. Finally, our results call for an update of the theory predictions with increased precision.

DOI: 10.1103/PhysRevD.105.116022

I. INTRODUCTION

Although the standard model (SM) of elementary particle physics can describe the subatomic world accurately, there are several theoretical and experimental indications that it needs to be completed. In general, precision tests of symmetries and their violation patterns provide guidelines toward a deeper understanding of elementary particles and their interactions. Here, we focus on charge-conjugation parity (*CP*) violation as a means of teasing out new physics. It is well known that the *CP*-violating mechanism in the SM is not sufficient to explain the observed imbalance between matter and antimatter in our Universe as a dynamic effect [1]. On the other hand, the processes included in the SM are strong enough to wash out any initial imbalance before the electroweak phase transition [2,3]. Thus, a *CP* violation beyond the SM is required. In the quark sector, the existence of *CP* violation in the kaon and beauty meson systems is well established [4–6], and so far, most observations are consistent with the SM expectations. There are tensions like the $B \to \pi K$ decay puzzle which require further exploration [7]. The first *CP*-violating signal for charmed mesons, reported by the LHCb experiment [8], is at the upper edge of the SM prediction. As *CP*-violating effects are subtle, a detailed understanding requires a systematical mapping of various hadronic systems studied with complementary approaches.

In the strange-quark sector, one of the most sensitive probes of non-SM contributions is direct *CP* violation. The experimental result is given by the value $\mathrm{Re}(\epsilon'/\epsilon) = (16.6 \pm 2.3) \times 10^{-4}$ [9–11] determined from the decay amplitude ratios of K_L and K_S mesons into pion pairs,

$$\frac{\mathcal{A}(K_L \to \pi^+\pi^-)}{\mathcal{A}(K_S \to \pi^+\pi^-)} =: \epsilon + \epsilon' \quad \text{and}$$
$$\frac{\mathcal{A}(K_L \to \pi^0\pi^0)}{\mathcal{A}(K_S \to \pi^0\pi^0)} =: \epsilon - 2\epsilon'. \tag{1}$$

*Andrzej.Kupsc@physics.uu.se

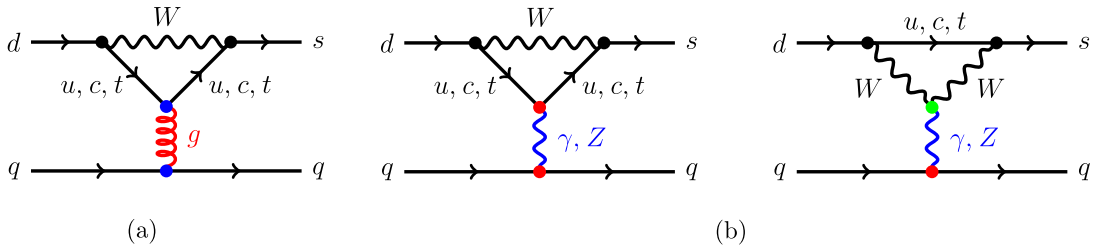

FIG. 1. Quark diagrams relevant for kaon and hyperon decays. Direct CP-violation effects in kaon and hyperon decays in the SM are given by the (a) QCD-penguin operators and (b) electroweak penguin operators. This figure was created using a modified script from Ref. [15].

This direct CP-violating effect arises in the weak part of the transition amplitudes to pions due to the interference between isospin $I = 0$ and $I = 2$ final states ($|\Delta I| = 1/2$ and $|\Delta I| = 3/2$ transitions, respectively). The CP-violation mechanism in the SM requires loop diagrams where all three quark families are involved, the so-called penguin diagrams, like those shown in Fig. 1. Predictions for the kaon decays have been a challenge for many years since there are partially canceling contributions from subleading types of the penguin diagrams, where the gluon line is replaced by γ, Z^0; see, e.g., Ref. [12] and references therein. Recently, a satisfactory understanding was reached using Lattice [13,14] and effective field theory [15,16] approaches to QCD. This progress ensures that the kaon decays continue to be an important precision test of the SM.

The subject of our paper is a complementary approach to study CP violation (CPV) in two-body nonleptonic $\Delta S = 1$ transitions of hyperons [17–22]. For such weak two-body decays, one also needs an interference pattern: this time between parity-even and parity-odd decay amplitudes. These emerge from the spin degrees of freedom of the initial and final baryons. Since we will consider decays of a spin-1/2 baryon B to a spin-1/2 baryon b and a pion, the parity-even amplitude leads to a p-wave final state, while the parity-odd amplitude leads to an s-wave final state. The two amplitudes are denoted P and S, respectively. In the following, we will often write the decay generically as $D(B \to b\pi)$. When we need to be more specific, we use indices Λ and Ξ to denote $\Lambda \to p\pi^-$ and $\Xi^- \to \Lambda\pi^-$, respectively. The decay amplitude is

$$\mathcal{A} \sim S\sigma_0 + P\boldsymbol{\sigma}\cdot\hat{\mathbf{n}}, \tag{2}$$

where σ_0 is the 2×2 unit matrix, $\boldsymbol{\sigma} \coloneqq (\sigma_1, \sigma_2, \sigma_3)$ are the Pauli matrices, and $\hat{\mathbf{n}} = \mathbf{q}/|\mathbf{q}|$ is the direction of the b-baryon momentum $\mathbf{q}$ in the B-baryon rest frame. It is important to note that these amplitudes depend on the initial (weak) decay, which produces the two final particles, but depend also on the (strong) final-state interaction. These S and P amplitudes are Lorentz scalars, which can depend only on the invariant mass of the two-body system. Yet, this quantity is fixed for a two-body decay: if we disregard the unmeasurable overall phase, the two complex amplitudes S and P can be fully specified by the overall normalization $|S|^2 + |P|^2$ and the size and relative phase of the interference term S^*P. These are directly related to the partial decay width and the following two parameters [23]:

$$\alpha_D \coloneqq \frac{2\mathrm{Re}(S^*P)}{|S|^2 + |P|^2} \quad \text{and} \quad \beta_D \coloneqq \frac{2\mathrm{Im}(S^*P)}{|S|^2 + |P|^2}. \tag{3}$$

The relation of the parameters to the shape of the angular distribution, including the polarization, of the baryon b will be shown in Sec. II. In the CP-conserving limit, the amplitudes $\bar{S}$ and $\bar{P}$ for the charge-conjugated (c.c.) decay mode of the antibaryon $\bar{D}(\bar{B} \to \bar{b} + \bar{\pi})$ are $\bar{S} = -S$ and $\bar{P} = P$. Therefore, the decay parameters have the opposite values: $\bar{\alpha}_D = -\alpha_D$ and $\bar{\beta}_D = -\beta_D$.

Two independent experimental CPV tests can be defined using these parameters,

$$A_{\mathrm{CP}}^D \coloneqq \frac{\alpha_D + \bar{\alpha}_D}{\alpha_D - \bar{\alpha}_D} \quad \text{and} \quad B_{\mathrm{CP}}^D \coloneqq \frac{\beta_D + \bar{\beta}_D}{\alpha_D - \bar{\alpha}_D}, \tag{4}$$

where $A_{\mathrm{CP}}^D(B_{\mathrm{CP}}^D) \neq 0$ indicates CP violation in the D decay. The A_{CP}^D test requires measurement of the angular $b(\bar{b})$ distribution from polarized $B(\bar{B})$-baryon decay. The B_{CP}^D test probes time-reversal-odd transitions and can be potentially much more sensitive, but it requires in addition a measurement of the $b(\bar{b})$-baryon polarization. In the SM, CPV effects in the hyperon decays are dominated by the QCD-penguin contribution, Fig. 1(a).

In the 1960s, hyperon decays were a tool for discrete symmetry tests on equal footing with the kaons. The last dedicated program to observe CP violation in hyperons was performed by the Fermilab experiments E756 [24] and HyperCP [25] at the dawn of this century. In these experiments, the sum of the A_{CP} observables for $\Xi^- \to \Lambda\pi^-$ ($[\Xi-]$) and $\Lambda \to p\pi^-$ ($[\Lambda p]$), $A_{\mathrm{CP}}^{[\Xi-]} + A_{\mathrm{CP}}^{[\Lambda p]}$, was studied. Here, the SM prediction amounts to $-0.5 \times 10^{-4} \leq A_{\mathrm{CP}}^{[\Xi-]} + A_{\mathrm{CP}}^{[\Lambda p]} \leq 0.5 \times 10^{-4}$ [26]. The published result $A_{\mathrm{CP}}^{[\Xi-]} + A_{\mathrm{CP}}^{[\Lambda p]} = 0(7) \times 10^{-4}$ [27] is currently considered to be the most precise test of CP symmetry in the hyperon sector.

TABLE I. Illustration of the expected statistical uncertainty for the CPV observables $A_{\mathrm{CP}}^{[\Lambda p]}$, $A_{\mathrm{CP}}^{[\Xi^-]}$, and $B_{\mathrm{CP}}^{[\Xi^-]}$ at BESIII and the proposed SCTF electron-positron collider. The results of the published BESIII measurements are given in the first row [31,32]. The uncertainties given in the two remaining rows are straightforward rescaling based on the expected number of events. The SM prediction for $A_{\mathrm{CP}}^{[\Lambda p]}$ is $\sim(1\text{–}5)\times 10^{-5}$, while for $B_{\mathrm{CP}}^{[\Xi^-]}$, it amounts to $\mathcal{O}(10^{-4})$ [26].

	$\sigma(A_{\mathrm{CP}}^{[\Lambda p]})$	$\sigma(A_{\mathrm{CP}}^{[\Xi^-]})$	$\sigma(B_{\mathrm{CP}}^{[\Xi^-]})$	Comment
BESIII	1.0×10^{-2}[a]	1.3×10^{-2}	3.5×10^{-2}	1.3×10^{9} J/ψ [31,32]
BESIII	3.6×10^{-3}	4.8×10^{-3}	1.3×10^{-2}	1.0×10^{10} J/ψ (projection)
SCTF	2.0×10^{-4}	2.6×10^{-4}	6.8×10^{-4}	3.4×10^{12} J/ψ (projection)

[a]This result is a combination of the two BESIII measurements.

The prospect of significantly improving the CPV tests in hyperons is due to a novel method where hyperon-antihyperon pairs are produced in electron-positron collisions at the c.m. energy corresponding to the J/ψ resonance. The J/ψ decays into a hyperon-antihyperon pair have relatively large branching fractions of $\mathcal{O}(10^{-3})$ [28]. The produced hyperon-antihyperon pair has a well-defined spin-entangled state based on the two possible partial waves (parity symmetry in this strong decay allows for an s and a d wave) [29,30]. The charge-conjugated decay modes of the hyperon and antihyperon can be measured simultaneously, and their properties can be compared directly. The uncertainties obtained in the proof-of-concept experiment [31,32] based on 1.3×10^{9} J/ψ for the $A_{\mathrm{CP}}^{[\Lambda p]}$, $A_{\mathrm{CP}}^{[\Xi^-]}$, and $B_{\mathrm{CP}}^{[\Xi^-]}$ observables are given in the first row of Table I. With the already available dataset of 10^{10} J/ψ collected at BESIII [33], a significantly improved statistical precision is expected, as shown in the second row of the table. However, the uncertainty is still predicted to be 2 orders of magnitude larger compared to the SM CPV signal.

Crucial improvements are expected at the next-generation electron-positron colliders, the super-charm-tau or super-tau-charm factories (SCTFs) being under consideration in China [34] and in Russia [35]. Their design luminosity is 2 orders of magnitude larger than the BEPCII collider [36,37], allowing for data samples of more than 10^{12} J/ψ events. The projections for the improved statistical uncertainties of the CPV tests, due to the increased data samples, are shown in Table I. This will still not be sufficient to observe an effect if it has a magnitude consistent with the SM predictions. Therefore, besides the increased luminosity, two additional improvements are being discussed to further increase the precision: (1) a c.m. energy spread ΔE compensation and (2) an electron beam polarization. For the first option, a collision scheme is proposed where electrons (positrons) with higher momenta are matched with positrons (electrons) with lower momenta. This promises a ΔE reduction to better match the natural width of J/ψ meson of $\Gamma = 0.09$ MeV, thus up to an order of magnitude increase of the number of J/ψ events for a given integrated luminosity [38–40]. For the second option, an electron beam polarization of 80%–90% at J/ψ energies can be obtained with the same beam current [41].

Since the benefits of the first improvement are obvious, we focus on the impact of the use of a polarized electron beam and show that the precision of the CP tests in $e^+e^- \to J/\psi \to \Lambda\bar{\Lambda}$ and $e^+e^- \to J/\psi \to \Xi\bar{\Xi}$ can be significantly improved. The initial findings for $e^+e^- \to J/\psi \to \Lambda\bar{\Lambda}$ have already been reported at the SCTF workshop [42] and independently in Ref. [43]. Here, we give a detailed explanation of this result and extend it to sequential hyperon weak decays. In Sec. II, we review the phenomenology and the current experimental status of CP tests in two-body weak decays of hyperons. In Sec. III, we use the formalism based on Jacob-Wick's [44] helicity amplitudes [45] to derive the hyperon-antihyperon production spin-correlation matrix for electron-positron collisions with longitudinal polarization of the electron beam. The asymptotic maximum log-likelihood method from Ref. [46] used for the analysis of uncertainties for the CPV observables is introduced in Sec. III C. The single-step decays are discussed in Sec. IV, and the two-step decays are discussed in Sec. V. Further experimental considerations are presented in Sec. VI, and Sec. VII contains an outlook.

II. *CP* TESTS IN HYPERON DECAYS

A. General considerations

There are three independent observables that provide a complete description of a weak decay $D(B \to b + \pi)$ with the amplitude given in Eq. (2). The first is the partial decay width given by

$$\Gamma = \frac{|\mathbf{q}|}{4\pi M_B}(E_b + M_b)|\mathcal{A}|^2, \tag{5}$$

where $|\mathcal{A}|^2 = |S|^2 + |P|^2$ and $E_b = \sqrt{|\mathbf{q}|^2 + M_b^2}$. The M_B and M_b are the masses of the mother and daughter baryons, respectively. The first of the two parameters defined in Eq. (3), $-1 < \alpha_D < 1$, can be determined from the angular distribution of the daughter baryon when the mother baryon

TABLE II. Properties of two-body hadronic decays of the ground-state octet hyperons. Branching fractions $\mathcal{B}$ are rounded to $\pm 0.5\%$ accuracy. In bold are the values assumed in this report. The motivation for the selection of the specific values is given in the main text.

	D	$\mathcal{B}$	$\langle\alpha_D\rangle$	$\langle\phi_D\rangle$ (rad)	$A_{\rm CP}$	Comment
$\Lambda \to p\pi^-$	$[\Lambda p]$	64%	$\mathbf{0.755(03)}$[a]	$\mathbf{-0.113(61)}$[b]	$\mathbf{-0.005(10)}$[a]	
			0.754(3)(2)	⋯	−0.006(12)(7)	BESIII [31]
			0.721(6)(5)*	⋯	⋯	CLAS [47]
			0.760(6)(3)	⋯	−0.004(12)(9)	BESIII [32]
$\Lambda \to n\pi^0$	$[\Lambda n]$	36%	$\mathbf{0.692(17)}$[c]	⋯	⋯	BESIII [31]
$\Sigma^+ \to p\pi^0$	$[\Sigma p]$	52%	$\mathbf{-0.994(04)}$[d]	$\mathbf{0.63(59)}$[g]	$\mathbf{-0.004(37)}$[d]	
$\Sigma^+ \to n\pi^+$	$[\Sigma n]$	48%	$\mathbf{0.068(13)}$*	$\mathbf{2.91(35)}$*	⋯	PDG [28]
$\Sigma^- \to n\pi^-$	$[\Sigma-]$	100%	$\mathbf{-0.068(08)}$*	$\mathbf{0.17(26)}$*	⋯	PDG [28]
$\Xi^0 \to \Lambda\pi^0$	$[\Xi 0]$	100%	$\mathbf{-0.345(08)}$[e]	$\mathbf{0.36(21)}$*	⋯	AVG [48,49]
$\Xi^- \to \Lambda\pi^-$	$[\Xi-]$	100%	$\mathbf{-0.379(04)}$[f]	−0.042(16)*	⋯	AVG [28,50]
			−0.373(5)(2)	0.016(14)(7)	$\mathbf{0.006(13)(6)}$	BESIII [32]

*Solely based on the result for hyperons (not antihyperons).
[a]Weighted average of the results from Refs. [31,32].
[b]Weighted average of $\phi_{[\Lambda p]}$ from Refs. [51–53], the same as in PDG [28].
[c]The $-\bar{\alpha}_{[\Lambda n]}$ value from Ref. [31].
[d]Value from Ref. [54].
[e]From $\alpha_{[\Xi 0]}\alpha_{[\Lambda p]} = -0.261(6)$ [28] divided by $\alpha^{\rm a}_{[\Lambda p]}$.
[f]Combination of $\langle\alpha_{[\Xi-]}\rangle$ [32] and $\alpha_{[\Xi-]}\alpha_{[\Lambda p]} = -0.294(5)$ [28] divided by $\alpha^{\rm a}_{[\Lambda p]}$.
[g]Weighted average of $\phi_{[\Sigma p]}$ from Refs. [55,56].

is polarized. For example, the proton angular distribution from the $\Lambda(\Lambda \to p\pi^-)$ decay in the Λ rest frame is given as

$$\frac{1}{\Gamma}\frac{d\Gamma}{d\Omega} = \frac{1}{4\pi}(1 + \alpha_\Lambda \mathbf{P}_\Lambda \cdot \hat{\mathbf{n}}), \tag{6}$$

where $\mathbf{P}_\Lambda$ is the Λ polarization vector. The second independent decay parameter can be chosen as the angle ϕ_D, $-\pi < \phi_D < \pi$, which gives the rotation of the spin vector between the B and b baryons. To measure ϕ_D, the polarization of both the mother and daughter baryons must be determined. For the decay $\Xi(\Xi^- \to \Lambda\pi^-)$, where the cascade is polarized, the ϕ_D parameter can be determined from the subsequent $\Lambda \to p\pi^-$ decay, which acts as a polarimeter. The relation between the initial Ξ^- polarization $\mathbf{P}_\Xi$ and the daughter Λ polarization $\mathbf{P}_\Lambda$ is given by the Lee-Yang formula [23],

$$\mathbf{P}_\Lambda = \frac{(\alpha_\Xi + \mathbf{P}_\Xi \cdot \hat{\mathbf{n}})\hat{\mathbf{n}} + \beta_\Xi \mathbf{P}_\Xi \times \hat{\mathbf{n}} + \gamma_\Xi \hat{\mathbf{n}} \times (\mathbf{P}_\Xi \times \hat{\mathbf{n}})}{1 + \alpha_\Xi \mathbf{P}_\Xi \cdot \hat{\mathbf{n}}}, \tag{7}$$

where the β- and γ-type decay parameters are expressed as

$$\begin{aligned} \beta_D &= \sqrt{1-\alpha_D^2}\sin\phi_D, \\ \gamma_D &:= \frac{|S|^2 - |P|^2}{|S|^2 + |P|^2} = \sqrt{1-\alpha_D^2}\cos\phi_D, \end{aligned} \tag{8}$$

implying that $\alpha_D^2 + \beta_D^2 + \gamma_D^2 = 1$. In Table II, the branching fractions ($\mathcal{B}$) and the values of the α_D and ϕ_D parameters for decays of the ground-state octet baryons are listed. When available, we report the hyperon-antihyperon average values, defined as

$$\langle\alpha_D\rangle = \frac{\alpha_D - \bar{\alpha}_D}{2}, \qquad \langle\phi_D\rangle = \frac{\phi_D - \bar{\phi}_D}{2}. \tag{9}$$

In most cases, the parameters of the antihyperon decays have not been determined yet. The α_D parameter is much easier to measure than ϕ_D, since only the polarization of the initial or final baryon has to be determined. Before 2018, the consensus was that the α_D parameters were known accurately. The BESIII measurement [31,32] has shown that values for $\Lambda \to p\pi^-$ and $\Xi^- \to \Lambda\pi^-$ were wrong by 17%.

The use of α_D and β_D parameters provides a symmetric description of the real and imaginary parts of the S and P amplitudes. On the other hand, the preferred choice of the α_D and ϕ_D parameters by the Particle Data Group (PDG) is motivated experimentally, as the ϕ_D and α_D uncertainties are approximately uncorrelated. However, the ϕ_D parameter is not directly related to the relative phase between the S and P amplitudes, since it can be written as

$$\phi_D = \arg\{(S+P)(S^* - P^*)\}. \tag{10}$$

In general, we do not need to know the exact values of the decay parameters to predict the uncertainties of the CPV observables given in Eq. (4). Many of our results can be described using approximate analytic formulas where the dependence on parameters is given explicitly. Furthermore, in the proposed measurements, the values of the decay parameters are determined directly together with the CPV observables and are uncorrelated with each other. For specific purposes, such as the estimate of the size of the decay amplitudes in Appendix A, we need the most precise values of the decay parameters and branching ratios or

lifetimes. We have made a critical evaluation of the available data, and the preferred values which we have selected are given in bold in Table II. Here, we provide a detailed explanation how some values were determined:

(i) The $\langle\alpha_{[\Lambda p]}\rangle$ value is the average of the two BESIII measurements [31,32]. We do not include the result from CLAS experiment [47] since it does not report the measurement of $\langle\alpha_{[\Lambda p]}\rangle$ and would indicate significant violation of the CP symmetry due to the statistically inconsistent value with the BESIII measurement of the antihyperon $\bar{\alpha}_{[\Lambda p]}$. The BESIII results for α_D and $\bar{\alpha}_D$ are correlated and have large uncertainty separately.

(ii) Since the $\langle\phi_{[\Xi-]}\rangle$ measured at BESIII [32] differs by 2.6 standard deviations from $\phi_{[\Xi-]}$ measured by HyperCP [50], we do not provide the average value for $\langle\phi_{[\Xi-]}\rangle$.

In addition, we will use other results which do not fit to the format of the table, such as $B_{\rm CP}^{[\Xi-]}$, $A_{\rm CP}^{[\Xi-]}+A_{\rm CP}^{[\Lambda p]}$, or life times of the cascades. They are introduced and referred to when we need to use them. For example, for the determination of the contribution of the $\Delta I=3/2$ amplitudes, we use more precise values of the branching fractions from Ref. [28]: $\mathcal{B}(\Lambda\to p\pi^-)=0.639(5)$ and $\mathcal{B}(\Lambda\to n\pi^0)=0.358(5)$.

B. CP-violation phenomenology

Isospin is not conserved in weak transitions, meaning that both the isospin vector length and the third component I_3 change in the decay process. In our hyperon decays of interest, there is effectively a transition from a strange to a down quark: thus, I_3 changes by $-1/2$. For the total isospin, the situation is more involved. It is convenient to classify the weak transition by the isospin ΔI of the transition operator. Starting with the initial isospin $I_{\rm ini}$ of the decaying hyperon, the isospin I of the final state can take values between $|I_{\rm ini}-\Delta I|$ and $I_{\rm ini}+\Delta I$. As a result of these considerations, it is practical to characterize the weak process by the isospin of the final state I and by the change of isospin ΔI. To explain this distinction, let us consider the process $\Xi^-\to\Lambda\pi^-$ where the initial and final isospins are $1/2$ and 1, respectively. This final state can be reached by a transition with $\Delta I=1/2$, where the isospins are aligned, and a transition with $\Delta I=3/2$, where the isospins are antialigned. Therefore, the transition amplitudes of the decomposition should be labeled by both I and ΔI, and we adopt the notation $S_{2\Delta I,2I}$ and $P_{2\Delta I,2I}$.

The transition amplitudes $L=S,P$ can be decomposed as [22]

$$L=\sum_j L_j\exp\{i(\xi_j^L+\delta_j^L)\},\tag{11}$$

where j represents a possible $\{2\Delta I,2I\}$ combination, while ξ_j^L and δ_j^L denote the weak CP-odd phase and the phase of the combined strong and electromagnetic (EM) final-state interaction, respectively, and the explicit expressions in the Λ and Ξ cases are written down in Eqs. (A6) and (A7). Appendixes B and C provide a justification for the decomposition in Eq. (11), where the S_j and P_j amplitudes are real numbers. The final-state interaction phase is dominated by the phase shifts of the strong elastic rescattering. The isospin-breaking effects in the rescattering due to hadron mass differences for different charge states are a few percent. Further contributions can be due to m_d-m_u terms in the amplitudes and EM interactions of the hadrons, such as radiative corrections or Coulomb interactions. The δ_j^L phase can be written as $\delta_j^L=\delta_{2I}^L+\Delta\delta_j^L$, where the correction term $\Delta\delta_j^L$ includes the isospin-breaking effects due to EM interactions in the final state. Here, we will neglect this term, but for future precision studies, it should be considered similar to how it was for the kaon to two-pion decays [57].

For the N–π final states, the phases shifts δ_{2I}^L are well known. We summarize in Table III the values from Ref. [58] which are relevant for the Λ and Σ decays. The $\Lambda-\pi$ scattering phase shifts, on the other hand, are less precisely determined from experiment. In particular, for $\Xi\to\Lambda\pi$, they can be found via the relation $\tan(\delta_2^P-\delta_2^S)=\sin\phi_\Xi\sqrt{1-\alpha_\Xi^2}/\alpha_\Xi$, neglecting the weak-phase difference, where α_Ξ and ϕ_Ξ are obtainable directly from the sequential decays. In doing so, we note that the current ϕ_Ξ data are not all consistent with each other yet, as pointed out in the preceding subsection. On the theoretical side, various analyses have produced different results [59–65], the latest one being $\delta_2^P-\delta_2^S=8.8(2)^\circ$ [65], which is compatible with one of the earlier predictions [63] and will be used in updating the $A_{\rm CP}^{[\Xi-]}$ prediction.

Now, we discuss signatures of CP violations in the hyperon decays. They are based on the comparison of the hyperon decay amplitudes, Eq. (11), with the ones corresponding to the antihyperon c.c. decay,

$$\bar{S}=-\sum_j S_j\exp\{i(-\xi_j^S+\delta_{2I}^S)\}\quad\text{and}$$
$$\bar{P}=\sum_j P_j\exp\{i(-\xi_j^P+\delta_{2I}^P)\},\tag{12}$$

where the real-number parameters L_j, ξ_j^L and δ_{2I}^L, $(L=S,P)$, have the same values for the hyperon and antihyperon

TABLE III. Values of the N–π scattering phase shifts δ_{2I}^L relevant for Λ and Σ decays from [58].

	$\lvert\mathbf{q}\rvert$ (MeV/c)	δ_1^S (°)	δ_3^S (°)	δ_1^P (°)	δ_3^P (°)
$\Lambda\to N\pi$	103	6.52(9)	−4.60(7)	−0.79(8)	−0.75(4)
$\Sigma\to N\pi$	190	9.98(23)	−10.70(13)	−0.04(33)	−3.27(15)

decays. The isospin-decomposition relations obtained in Appendix A can be applied to the c.c. decays of anti-hyperons. *A priori*, up to three independent observables can be used to compare properties of a decay to the c.c. one. The first observable is the difference between the partial decay widths

$$\Delta_{\rm CP} \coloneqq \frac{\Gamma - \bar{\Gamma}}{\Gamma + \bar{\Gamma}}. \tag{13}$$

In the $\Delta I = 1/2$ limit, the $\Delta_{\rm CP}$ observable is exactly zero and cannot be used to test CP symmetry. In addition, for $\Xi \to \Lambda\pi$, the isospin of the final Λ–π state is $I = 1$, and there is only one strong phase for each of the S and P amplitudes. This implies that the corresponding $\Delta_{\rm CP}$ is zero even if the weak transition includes $|\Delta I| = 3/2$ operators. However, the $\Delta_{\rm CP}$ test is possible for $\Lambda \to N\pi$, as the final state can have $I = 1/2$ or $3/2$. For the two Λ-decay modes, to lowest order in the $\Delta I = 3/2$ amplitudes, starting from Eq. (A6), we have the relation $2\Delta_{\rm CP}^{[\Lambda p]} = -\Delta_{\rm CP}^{[\Lambda n]} = 2\sqrt{2}\Delta_{\rm CP}$ with

$$\Delta_{\rm CP} = \frac{P_{1,1}P_{3,3}\sin(\xi^P_{1,1} - \xi^P_{3,3})\sin(\delta^P_1 - \delta^P_3) + S_{1,1}S_{3,3}\sin(\xi^S_{1,1} - \xi^S_{3,3})\sin(\delta^S_1 - \delta^S_3)}{P^2_{1,1} + S^2_{1,1}}. \tag{14}$$

This requires two weak and two strong phases either in the S amplitude, as in the kaon decays, or in the P amplitude. The precision of the test is suppressed by the small $|\Delta I| = 3/2$ amplitudes and by the term containing the sinus of the small strong phases. Therefore, such a test is not competitive, and we will not discuss it further.

The remaining two CP tests involve the $A^D_{\rm CP}$ and $B^D_{\rm CP}$ observables defined in Eq. (4). If one works to leading order in the weak phases, $B^D_{\rm CP}$ can also be expressed as

$$B^D_{\rm CP} = \Phi^D_{\rm CP}\frac{\sqrt{1 - \langle\alpha_D\rangle^2}}{\langle\alpha_D\rangle}\cos\langle\phi_D\rangle - A^D_{\rm CP}\frac{\langle\alpha_D\rangle}{\sqrt{1 - \langle\alpha_D\rangle^2}}\sin\langle\phi_D\rangle, \tag{15}$$

where $\langle\alpha_D\rangle$ and $\langle\phi_D\rangle$ were defined in Eq. (9) and

$$\Phi^D_{\rm CP} \coloneqq \frac{\phi_D + \bar{\phi}_D}{2} \tag{16}$$

is based on the spin-rotation decay parameter ϕ_D. In a large acceptance experiment, the decay parameters α and ϕ are uncorrelated, as are the CPV tests based on the $A^D_{\rm CP}$ and $\Phi^D_{\rm CP}$ variables.

Contrary to the CP violation in $K_{L,S} \to \pi\pi$, where $\Delta I = 1/2$ and $\Delta I = 3/2$ amplitudes are both consequential, the dominant effect in hyperons can be studied using only the $\Delta I = 1/2$ amplitudes. The corrections to the CPV effect studied in this approximation will be a few percent, as given by the size of the P_3 and S_3 amplitudes. This is sufficient for the precision expected at SCTF. If a better precision is required, one can construct isospin averages of the observables from different isospin modes to recover the results in the $\Delta I = 1/2$ limit. Such averages are constructed from the isospin decomposition of a given decay process (channel)—for more details, we refer to Appendix A. For Ξ, up to the linear terms in the $\Delta I = 3/2$ amplitudes, they amount to

$$B^\Xi_{\rm CP} \coloneqq \frac{2B^{[\Xi-]}_{\rm CP} + B^{[\Xi0]}_{\rm CP}}{3} = \tan(\xi^P_{1,2} - \xi^S_{1,2}), \tag{17}$$

$$A^\Xi_{\rm CP} \coloneqq \frac{2A^{[\Xi-]}_{\rm CP} + A^{[\Xi0]}_{\rm CP}}{3} = -\tan(\xi^P_{1,2} - \xi^S_{1,2})\tan(\delta^P_2 - \delta^S_2), \tag{18}$$

and for Λ,

$$B^\Lambda_{\rm CP} \coloneqq \frac{2B^{[\Lambda p]}_{\rm CP} + B^{[\Lambda n]}_{\rm CP}}{3} = \tan(\xi^P_{1,1} - \xi^S_{1,1}), \tag{19}$$

$$A^\Lambda_{\rm CP} \coloneqq \frac{2A^{[\Lambda p]}_{\rm CP} + A^{[\Lambda n]}_{\rm CP}}{3} = -\tan(\xi^P_{1,1} - \xi^S_{1,1})\tan(\delta^P_1 - \delta^S_1). \tag{20}$$

The leading-order correction for the two isospin states of the cascades is

$$\begin{aligned} B^{[\Xi-]}_{\rm CP} - B^{[\Xi0]}_{\rm CP} &= -\frac{3}{2}\left[\frac{P_{3,2}}{P_{1,2}}\sin(\xi^P_{1,2} - \xi^P_{3,2}) - \frac{S_{3,2}}{S_{1,2}}\sin(\xi^S_{1,2} - \xi^S_{3,2})\right], \\ A^{[\Xi-]}_{\rm CP} - A^{[\Xi0]}_{\rm CP} &= -(B^{[\Xi-]}_{\rm CP} - B^{[\Xi0]}_{\rm CP})\tan(\delta^P_2 - \delta^S_2), \end{aligned} \tag{21}$$

which implies that, even if the LO $\Delta I = 3/2$ corrections are included, the A and B tests are still connected—giving the same combination of the weak phases. For the Λ decays,

such a relation is not valid, and the A- and B-type variables provide independent information on the weak-phase combinations. We will not discuss this case, since the B-type observables cannot be measured with the standard techniques available at the electron-positron collider experiments. A combination of the CP tests for the isospin related channels allows for an increased statistical significance of the tests. Such an approach is feasible at SCTF for the Ξ and Λ decays, since all the decay parameters for (anti) cascade and the α parameters for Λ can be measured.

A simpler approach is to treat each decay mode separately when comparing decay parameters for the hyperon and, from the c.c. decay, for the antihyperon. In the $\Delta I = 1/2$ approximation, we can write

$$\begin{aligned} S &= |\mathcal{A}| \sin\zeta \exp(i\xi_S + i\delta_S), \\ \bar{S} &= -|\mathcal{A}| \sin\zeta \exp(-i\xi_S + i\delta_S), \\ P &= |\mathcal{A}| \cos\zeta \exp(i\xi_P + i\delta_P), \\ \bar{P} &= |\mathcal{A}| \cos\zeta \exp(-i\xi_P + i\delta_P), \end{aligned} \tag{22}$$

where $0 \le \zeta \le \pi$, $\xi_S(\xi_P)$ is the weak CP-odd phase for the $\Delta I = 1/2$ transition and $\delta_S(\delta_P)$ is the strong $s(p)$-wave baryon-pion phase shift at the c.m. energy corresponding to the hyperon mass. The structure of Eq. (22) can be justified, if one assumes that the complete decay process can be split up into the decay itself where one does not resolve the intrinsic structure and a final-state interaction that conserves P and C separately. If one does not resolve the space-time structure of the initial decay, then one can use an effective Hermitian Lagrangian to describe the decay, and one just reads off the relations $\bar{S}_{\rm ini} = -S^*_{\rm ini}$ and $\bar{P}_{\rm ini} = P^*_{\rm ini}$. More details are given in Appendix B. The final-state interaction can be described by a 4×4 Omnès-function matrix that is applied to the four initial amplitudes; see also Appendix C. If P (and baryon number) is conserved, then this matrix is diagonal. If C is conserved, then the entries are pairwise the same for the particle and antiparticle. Without inelasticities, Watson's theorem [66] identifies the phases with the scattering phase shifts. The decay parameters (α, β, γ) and $(\bar{\alpha}, \bar{\beta}, \bar{\gamma})$[1] are then given as

$$\begin{aligned} \alpha &= \sin(2\zeta)\cos(\xi_P - \xi_S + \delta_P - \delta_S), \\ \bar{\alpha} &= -\sin(2\zeta)\cos(-\xi_S + \xi_P + \delta_S - \delta_P), \end{aligned} \tag{23}$$

$$\begin{aligned} \beta &= \sin(2\zeta)\sin(\xi_P - \xi_S + \delta_P - \delta_S), \\ \bar{\beta} &= -\sin(2\zeta)\sin(-\xi_P + \xi_S + \delta_P - \delta_S), \end{aligned} \tag{24}$$

$$\gamma = -\cos(2\zeta), \qquad \bar{\gamma} = -\cos(2\zeta). \tag{25}$$

[1]In the remaining part of this section, we simplify the notation by omitting subscript D for the decay parameters.

Without final-state interactions, $\alpha + \bar{\alpha}$ is always zero, and $A_{\rm CP}$ does not constitute an observable that can indicate CP violation, while $B_{\rm CP} = \tan(\xi_P - \xi_S)$ does. One needs CP violation and final-state interactions to make $A_{\rm CP}$ different from zero. In the presence of final-state interactions, $\beta \neq 0$ does not necessarily indicate CP violation, but $B_{\rm CP}$ still does. The CPV tests based on the $A_{\rm CP}$ and $B_{\rm CP}$ (and $\Phi_{\rm CP}$) observables can be expressed using Eq. (22) as

$$A_{\rm CP} = -\frac{\sqrt{1-\alpha^2}}{\alpha}\sin\phi\tan(\xi_P - \xi_S) \tag{26}$$

$$= -\tan(\delta_P - \delta_S)\tan(\xi_P - \xi_S), \tag{27}$$

$$B_{\rm CP} = \tan(\xi_P - \xi_S), \tag{28}$$

$$\Phi_{\rm CP} = \frac{\alpha}{\sqrt{1-\alpha^2}}\cos\phi\tan(\xi_P - \xi_S). \tag{29}$$

Therefore, the tests are not independent as they are related to the same $\xi_P - \xi_S$ combination of the CP-odd weak phases. For single-step decays of the singly strange baryons, measurement of the $B_{\rm CP}(\Phi_{\rm CP})$ would require a dedicated detector to determine the daughter-nucleon polarization. Therefore, for the Λ and Σ hyperon decays, we consider only the $A_{\rm CP}$ observable measurements. In this case, the weak phases are determined by Eq. (27) using the well-known values of the strong N–π phases. Since the strong phases δ_P and δ_S, representing the final-state interaction between the baryon and pion, are small, the $B_{\rm CP}$ observable provides much better determination of the weak-phase difference than $A_{\rm CP}$. This statement assumes that the uncertainties of the $A_{\rm CP}$ and $B_{\rm CP}$ (or $\Phi_{\rm CP}$) measurements are comparable. In Sec. VI, we will discuss strategies for the simultaneous measurement of the two observables in the cascade decays.

C. Status of the CPV predictions

In this subsection, we review the estimates of CPV signals for the decay channels $\Lambda \to p\pi^-$ and $\Xi^- \to \Lambda\pi^-$, commonly considered to be the most sensitive modes. In the experimental study of the latter, the former is used as the subsequent process. The SM contributions to $\xi_P - \xi_S$ for the two decay modes are shown in the third column of Table IV. These predictions are both $\mathcal{O}(10^{-4})$, taking into account the substantial uncertainties which are related to our present lack of ability to explain simultaneously the s and p waves of hyperon nonleptonic decays [26]. The second column of this table contains $\xi_P - \xi_S$ divided by $\eta\lambda^5 A^2$, which is a product of the Wolfenstein parameters for the Cabibbo-Kobayashi-Maskawa matrix and has a value of $1.36(7) \times 10^{-4}$ according to the most recent PDG report [28]. The SM entries in this table are updates of the corresponding numbers found in Ref. [26] and are somewhat modified with respect to the latter, mainly because of

TABLE IV. Weak-phase differences in hyperon decays. (left) Standard-model predictions and (right) parameters C_B and C'_B used in Eq. (30) to relate the weak-phase differences in hyperon decays to the beyond SM (BSM) constraints from kaon CPV observables. The SM and BSM entries are updates of the corresponding numbers obtained in Refs. [26,67], respectively, as explained in the main text.

	$\xi_P - \xi_S$			
	$(\eta\lambda^5 A^2)$	$[10^{-4}$ rad$]$	C_B	C'_B
	SM		BSM	
$\Lambda \to p\pi^-$	-0.1 ± 1.5	-0.2 ± 2.2	0.9 ± 1.8	0.4 ± 0.9
$\Xi^- \to \Lambda\pi^-$	-1.5 ± 1.2	-2.1 ± 1.7	-0.5 ± 1.0	0.4 ± 0.7

our use of the (boldfaced) new α results for $\Lambda \to p\pi^-$ and $\Xi^- \to \Lambda\pi^-$ quoted in Table II.

To compare the theoretical $A_{\rm CP}$ with its most precise measurements to date given in Table II requires multiplication of the calculated $\xi_P - \xi_S$ by the strong-interaction parameters, as indicated in Eqs. (26) and (27), an extra step which increases the experimental uncertainty and/or decreases the precision of the predictions. Nevertheless, from Eq. (28), we expect that future measurements of $B_{\rm CP}$ can directly determine $\xi_P - \xi_S$ with good precision. For $\Lambda \to p\pi^-$, the strong phases pertaining to Eq. (27) are $\delta_1^S = 0.11(2)$ rad and $\delta_1^P = -0.014(1)$ rad from Table III. For $\Xi^- \to \Lambda\pi^-$, the strong-phase difference can be extracted experimentally using the methods discussed in this paper. However, since $\beta_{[\Xi-]}$ is not yet well measured, the $\alpha_{[\Xi-]}$ data cannot be used to obtain $\delta_2^P - \delta_2^S$ with good precision via $\beta_{[\Xi-]} = \alpha_{[\Xi-]} \tan(\delta_2^P - \delta_2^S)$. To update the prediction for $A_{\rm CP}^{[\Xi-]}$, we adopt instead the theoretical value $\delta_2^P - \delta_2^S = 8.8(2)$ deg computed in Ref. [65]. Putting together the weak and strong phases, we then arrive at the SM ranges $-3 \times 10^{-5} \le A_{\rm CP}^{[\Lambda p]} \le 3 \times 10^{-5}$ and $0.5 \times 10^{-5} \le A_{\rm CP}^{[\Xi-]} \le 6 \times 10^{-5}$, which are below their respective experimental bounds inferred from Table II by more than 2 orders of magnitude.

Measurements on hyperon CPV and its kaon counterpart are complementary to each other because they do not probe the underlying physics in the same way. As mentioned above, in the context of the SM, the direct-CPV parameter ϵ' in the kaon decay $K \to \pi\pi$ arises from both $|\Delta I| = 1/2$ and $|\Delta I| = 3/2$ transitions, where the CP-odd phases come from the QCD, Fig. 1(a), and electroweak, Fig. 1(b), penguin contributions, respectively, all of which are induced by effective four-quark operators. There is a delicate balance and cancellation between the two contributions. In the hyperon case, the CPV signal of interest here, such as measured by $A_{\rm CP}$ or $B_{\rm CP}$, mainly comes from $|\Delta I| = 1/2$ transitions and is dominated by the QCD penguins.

In the presence of physics beyond the SM (BSM), there might be new ingredients causing other types of quark operators to appear and generate effects that are enhanced relative to the SM contributions. This possibility can be realized, for instance, by the so-called chromomagnetic-penguin operators, which contain a ds quark bilinear coupled to gluon fields and could be influenced by sizeable new physics in various models [67–72]. The parity-odd and parity-even portions of the operators contribute to ϵ' and the CPV parameter ϵ in neutral-kaon mixing, respectively, and both parts simultaneously affect $\xi_P - \xi_S$. Model independently, one can derive a general relation between the contributions of these operators to the hyperon weak-phase difference and kaon observables [67],

$$(\xi_P - \xi_S)_{\rm BSM} = \frac{C'_B}{B_G}\left(\frac{\epsilon'}{\epsilon}\right)_{\rm BSM} + \frac{C_B}{\kappa}\epsilon_{\rm BSM}, \qquad (30)$$

which further illustrates the complementarity of hyperon and kaon processes. The values of C_B and C'_B, updated from their counterparts evaluated in Ref. [67], are given in Table IV; B_G parametrizes the hadronic uncertainty, and κ quantifies the contribution of meson poles. The allowed ranges of $(\epsilon'/\epsilon)_{\rm BSM}$ and $\epsilon_{\rm BSM}$ can be estimated by comparing the experimental values of ${\rm Re}(\epsilon'/\epsilon)$ and $|\epsilon|$ with the recent SM predictions [73–75]. Following Ref. [75], we impose

$$\left|\frac{\epsilon'}{\epsilon}\right|_{\rm BSM} \le 1 \times 10^{-3}, \qquad |\epsilon|_{\rm BSM} \le 2 \times 10^{-4}. \qquad (31)$$

Accordingly, using $0.5 < B_G < 2$ and $0.2 < |\kappa| < 1$ [71], we find that the kaon data imply the limits $|\xi_P - \xi_S|_{\rm BSM}^{[\Lambda p]} \le 5.4 \times 10^{-3}$ and $|\xi_P - \xi_S|_{\rm BSM}^{[\Xi-]} \le 3.7 \times 10^{-3}$. Additionally, we arrive at $|A_{\rm CP}^{[\Lambda p]} + A_{\rm CP}^{[\Xi-]}|_{\rm BSM} \le 11 \times 10^{-4}$, and therefore the upper end of this range is already in tension with the aforementioned HyperCP limit [27]. Clearly, hyperon CPV measurements with much improved precision will provide an independent constraint on the BSM contributions in the strange quark sector. However, a lot also remains to be done on the theory side, as the predictions presently suffer from considerable uncertainties. It is hoped that lattice QCD analyses [76] in the future could help solve this problem.

D. Experimental status of CPV tests

The dedicated CPV experiment HyperCP (E871) at Fermilab [77], operating between 1996 and 1999, set the world's best upper limits on hyperon CP violation using the $\Xi^- \to \Lambda\pi \to p\pi^-\pi^-$ decay sequence. A secondary cascade beam was produced by having 800 GeV/c primary protons interacting with a copper target. The sum of the asymmetries $A_{\rm CP}^{[\Xi-]} + A_{\rm CP}^{[\Lambda p]} = 0(5)(4) \times 10^{-4}$ [27] was determined with a data sample of 117×10^6 Ξ^- and 41×10^6 $\bar{\Xi}^+$ using unpolarized cascades. A preliminary result $A_{\rm CP}^{[\Xi-]} + A_{\rm CP}^{[\Lambda p]} = -6(2)(2) \times 10^{-4}$ based on the full data sample of $862 \times 10^6\Xi$ and $230 \times 10^6\bar{\Xi}$ was presented at the BEACH2008

conference [78]. Since the final result was never published, one can suspect that an inherent problem in understanding the systematic effects at the level of 4×10^{-4} was found. The HyperCP has also measured the most precise value of $\phi_{[\Xi-]}$, see Table II, using 144×10^6 Ξ^- events with average polarization of ∼5% [50]. The drawback of the HyperCP experimental method is the charge-conjugation-asymmetric production mechanism and the need to use separate runs with different settings for the baryon and antibaryon measurements. Furthermore, the accuracy of the $\phi_{[\Xi-]}$ parameter determination was limited by the low value of the Ξ^--beam polarization.

The most recent results, marked by bold font in Table II, come from the proof-of-concept measurements [31,32,54] at BESIII using a novel method [45,46,79]. These results have been obtained using collisions of unpolarized electron and positron beams at the c.m. energy corresponding to the J/ψ resonance. The relevant properties of the $J/\psi \to B\bar{B}$ processes are given in Table V. Given the relatively large branching fractions and low hadronic background, these e^+e^- experiments are well suited for CPV tests. Two different analysis methods can be used: exclusive measurement [double tag (DT)], where the decay chains of the baryon and antibaryon are fully reconstructed, and inclusive measurement [single tag (ST)], where only the decay chain of the baryon or antibaryon is reconstructed. For the ST analysis, the two-body production process is uniquely identifiable, and its kinematics is fully determined using missing energy/mass technique. Of importance for all single-step weak decays, e.g., $\Lambda \to p\pi^-$, is that the Λ and $\bar{\Lambda}$ are produced with a transverse polarization. The polarization and the spin correlations allow for a simultaneous determination of α and $\bar{\alpha}$, with the method proposed in Ref. [79]. The currently available results for $J/\psi \to \Lambda\bar{\Lambda}$ [31], $J/\psi \to \Sigma^+\bar{\Sigma}^-$ [54], and $J/\psi \to \Xi^-\bar{\Xi}^+$ [32] use 1.3×10^9 J/ψ data with 4.2×10^5 (background 400 events), 8.8×10^4 (background 4.4×10^3 events), and 7.3×10^4 (background 200 events) selected DT candidates, respectively. The final-state charged particles are measured in the main drift chamber [and the calorimeter for the photons from the $\Sigma^+ \to p\pi^0(\to\gamma\gamma)$ decay], where a superconducting solenoid provides the magnetic field for momentum determination of the pions and (anti)protons with an accuracy of 0.5% at 1.0 GeV/c [37]. The pions and protons have distinctly different momentum ranges, making particle identification straightforward in the DT-type measurements. The analyses of the already collected 10^{10} J/ψ data by BESIII have not been finished yet, but one can expect a threefold reduction of the statistical uncertainties as shown in Table I.

TABLE V. Properties of the $e^+e^- \to J/\psi \to B\bar{B}$ decays to the pairs of ground-state octet hyperons.

Final state	$\mathcal{B}(\times 10^{-4})$	α_ψ	$\Delta\Phi$ (rad)	Comment
$\Lambda\bar{\Lambda}$	19.43(3)	0.461(9)	0.740(13)	[31,80]
$\Sigma^+\bar{\Sigma}^-$	15.0(24)	−0.508(7)	−0.270(15)	[54,81]
$\Sigma^-\bar{\Sigma}^+$	⋯	⋯	⋯	—no data—
$\Sigma^0\bar{\Sigma}^0$	11.64(4)	−0.449(20)	⋯	[80]
$\Xi^0\bar{\Xi}^0$	11.65(43)	0.66(6)	⋯	[82]
$\Xi^-\bar{\Xi}^+$	9.7(8)	0.586(16)	1.213(48)	[28,32]

III. FORMALISM

A. Production process

We start from a description of baryon-antibaryon production in electron-positron annihilations with a polarized electron beam. The production process $e^+e^- \to B\bar{B}$, viewed in the c.m. frame, defines the z axis, which is chosen along the positron momentum shown in Fig. 2. We consider production of a spin-1/2 baryon-antibaryon pair in electron-positron annihilation with a longitudinally polarized electron beam. Neglecting the electron mass and assuming the one-photon approximation, the helicities of the electron (λ) and positron ($\bar{\lambda}$) have to be opposite since the photon only couples right-handed particles to left-handed antiparticles and vice versa. The numbers of right-handed (n_R) and left-handed (n_L) electrons in the beam with longitudinal polarization P_e are

$$n_R = n_- \cdot \frac{1+P_e}{2} \quad \text{and} \quad n_L = n_- \cdot \frac{1-P_e}{2}, \tag{32}$$

where $n_- = n_R + n_L$ is the total number of electrons. The two helicity configurations where the annihilation is possible are $\lambda = +1/2, \bar{\lambda} = -1/2$ $(\lambda_z = -1)$ and $\lambda = -1/2, \bar{\lambda} = +1/2$ $(\lambda_z = 1)$. For the collisions with unpolarized positrons, the relative weights of the two configurations are $(1+P_e)/2$ and $(1-P_e)/2$, respectively. Therefore, the spin density of the initial electron-positron system can be written as

$$\rho_1^{i,j}(\theta) := \frac{1+P_e}{2} d^{1*}_{-1,i}(\theta) d^1_{-1,j}(\theta) + \frac{1-P_e}{2} d^{1*}_{1,i}(\theta) d^1_{1,j}(\theta), \tag{33}$$

where the quantization axis is along the B momentum. The density matrix for the production process is the sum of the

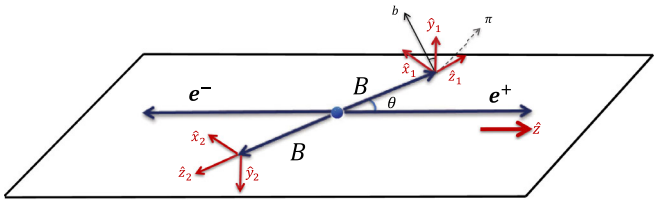

FIG. 2. Orientation of the three coordinate systems used in the analysis. The axes in the baryon B and antibaryon $\bar{B}$ rest (helicity) frames are $(\hat{\mathbf{x}}_1, \hat{\mathbf{y}}_1, \hat{\mathbf{z}}_1)$ and $(\hat{\mathbf{x}}_2, \hat{\mathbf{y}}_2, \hat{\mathbf{z}}_2)$, respectively. They are related as $(\hat{\mathbf{x}}_2, \hat{\mathbf{y}}_2, \hat{\mathbf{z}}_2) = (\hat{\mathbf{x}}_1, -\hat{\mathbf{y}}_1, -\hat{\mathbf{z}}_1)$. In the overall c.m. frame, the $\hat{\mathbf{z}}$ axis is along the positron momentum.

contributions from the two helicities (see Eq. (14) in Ref. [45])

$$\rho_{B\bar{B}}^{\lambda_1,\lambda_2;\lambda_1',\lambda_2'} \propto A_{\lambda_1,\lambda_2} A^*_{\lambda_1',\lambda_2'} \rho_1^{\lambda_1-\lambda_2,\lambda_1'-\lambda_2'}(\theta) \tag{34}$$

with the reduced density matrix ρ_1 given by

$$\frac{1}{2}\begin{pmatrix} \frac{1+\cos^2\theta}{2} - P_e\cos\theta & \frac{(P_e-\cos\theta)\sin\theta}{\sqrt{2}} & \frac{\sin^2\theta}{2} \\ \frac{(P_e-\cos\theta)\sin\theta}{\sqrt{2}} & \sin^2\theta & \frac{(P_e+\cos\theta)\sin\theta}{\sqrt{2}} \\ \frac{\sin^2\theta}{2} & \frac{(P_e+\cos\theta)\sin\theta}{\sqrt{2}} & \frac{1+\cos^2\theta}{2} + P_e\cos\theta \end{pmatrix}. \tag{35}$$

The four *a priori* possible helicity amplitudes reduce to only two, $h_1 := A_{-1/2,-1/2} = A_{1/2,1/2}$ and $h_2 := A_{1/2,-1/2} = A_{-1/2,1/2}$. If one focuses on the not normalized angular distribution of the production process, the relevant information contained in the two complex form factors h_1 and h_2 can be expressed using only two real parameters. Hence, disregarding the overall normalization, the magnitudes of the two form factors can be represented as $|h_1| = \cos\chi$ and $|h_2| = \sqrt{2}\sin\chi$, where $0 \le \chi \le \pi/2$. In addition, the relative phase between the form factors can be defined as $\Delta\Phi := \arg(h_1/h_2)$. The general expression for the joint density matrix of the $B\bar{B}$ pair is

$$\rho_{B\bar{B}} = \sum_{\mu,\nu=0}^{3} C_{\mu\nu}\sigma_\mu^B \otimes \sigma_\nu^{\bar{B}}, \tag{36}$$

where a set of four Pauli matrices $\sigma_\mu^B(\sigma_\nu^{\bar{B}})$ in the $B(\bar{B})$ rest frame is used and $C_{\mu\nu}$ is a 4×4 real matrix representing polarizations and spin correlations of the baryons. The orientation of the coordinate systems in the baryon rest frames is defined in Fig. 2. The axes are denoted as $\hat{\mathbf{x}}_1, \hat{\mathbf{y}}_1, \hat{\mathbf{z}}_1$ and $\hat{\mathbf{x}}_2, \hat{\mathbf{y}}_2, \hat{\mathbf{z}}_2$. The elements of the $C_{\mu\nu}$ matrix are functions of the production angle θ of the B baryon:

$$\frac{3}{3+\alpha_\psi}\cdot\begin{pmatrix} 1+\alpha_\psi\cos^2\theta & \gamma_\psi P_e\sin\theta & \beta_\psi\sin\theta\cos\theta & (1+\alpha_\psi)P_e\cos\theta \\ \gamma_\psi P_e\sin\theta & \sin^2\theta & 0 & \gamma_\psi\sin\theta\cos\theta \\ -\beta_\psi\sin\theta\cos\theta & 0 & \alpha_\psi\sin^2\theta & -\beta_\psi P_e\sin\theta \\ -(1+\alpha_\psi)P_e\cos\theta & -\gamma_\psi\sin\theta\cos\theta & -\beta_\psi P_e\sin\theta & -\alpha_\psi-\cos^2\theta \end{pmatrix}, \tag{37}$$

where the real parameters α_ψ, β_ψ, and γ_ψ are expressed in terms of the previously defined χ and $\Delta\Phi$ as

$$\alpha_\psi := -\cos(2\chi), \qquad \beta_\psi := \sin(2\chi)\sin(\Delta\Phi), \qquad \gamma_\psi := \sin(2\chi)\cos(\Delta\Phi) \tag{38}$$

and $\alpha_\psi^2 + \beta_\psi^2 + \gamma_\psi^2 = 1$. The B-baryon angular distribution is

$$\frac{1}{\sigma}\frac{d\sigma}{d\Omega_B} = \frac{3}{4\pi}\frac{1+\alpha_\psi\cos^2\theta}{3+\alpha_\psi}. \tag{39}$$

This relation determines the normalization factor in Eq. (37). The B-baryon polarization vector $\mathbf{P}_B$ defined in the rest frame of baryon B, coordinates $(\hat{\mathbf{x}}_1, \hat{\mathbf{y}}_1, \hat{\mathbf{z}}_1)$, is

$$\mathbf{P}_B := \frac{C_{10}\hat{\mathbf{x}}_1 + C_{20}\hat{\mathbf{y}}_1 + C_{30}\hat{\mathbf{z}}_1}{C_{00}} = \frac{\gamma_\psi P_e\sin\theta\hat{\mathbf{x}}_1 - \beta_\psi\sin\theta\cos\theta\hat{\mathbf{y}}_1 - (1+\alpha_\psi)P_e\cos\theta\hat{\mathbf{z}}_1}{1+\alpha_\psi\cos^2\theta}. \tag{40}$$

In the chosen helicity frames, one has $C_{01} = C_{10}$, $C_{02} = -C_{20}$, $C_{03} = -C_{30}$ and $\mathbf{P}_{\bar{B}} = (C_{01}\hat{\mathbf{x}}_2 + C_{02}\hat{\mathbf{y}}_2 + C_{03}\hat{\mathbf{z}}_2)/C_{00}$. Therefore, the polarization vectors of the baryon and the antibaryon are equal and have the same direction, $\mathbf{P}_{\bar{B}} = \mathbf{P}_B$. In the limit of large c.m. energies (HE), where $\alpha_\psi = 1$ and $\beta_\psi = \gamma_\psi = 0$ [83], the baryon can only have the longitudinal polarization component $\mathbf{P}_B\hat{\mathbf{z}}_1 = 2P_e\cos\theta/(1+\cos^2\theta)$. In the low energy (LE) limit (close to threshold), $\alpha_\psi = 0$ and $\Delta\Phi = 0$, implying $\beta_\psi = 0$, $\gamma_\psi = 1$, and $\mathbf{P}_B = P_e(\sin\theta\hat{\mathbf{x}}_1 + \cos\theta\hat{\mathbf{z}}_1)$. Therefore, the value of the baryon polarization is equal to the initial electron beam polarization in this case. Figure 3 shows the production-angle dependence of the baryon-polarization magnitude in the $e^+e^- \to J/\psi \to \Lambda\bar{\Lambda}$, $e^+e^- \to J/\psi \to \Xi^-\bar{\Xi}^+$ and $e^+e^- \to J/\psi \to \Sigma^+\bar{\Sigma}^-$

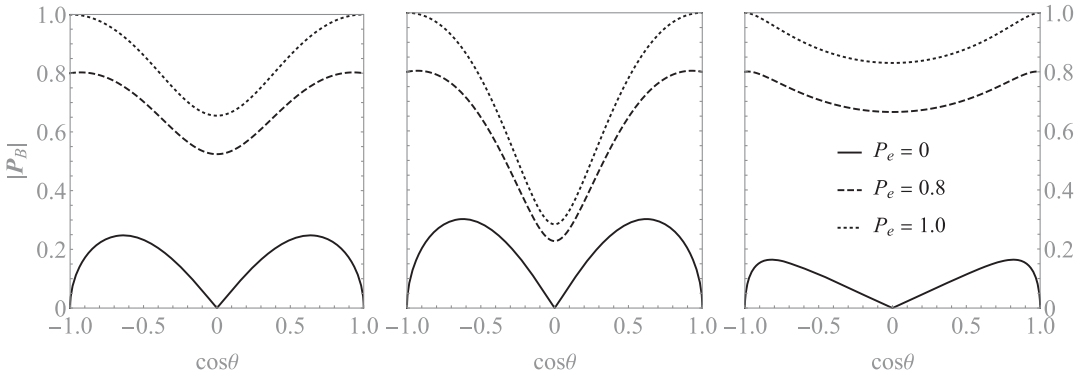

FIG. 3. Magnitudes of the hyperon polarization as a function of the production angle for (a) Λ, (b) Ξ^-, and (c) Σ^+ for the electron beam polarizations $P_e = 0$, 0.8, 1 (solid, dashed, and dotted lines, respectively). The α_ψ and $\Delta\Phi$ values are taken from Table V.

processes for three different values of the electron-beam polarization. The values of the α_ψ and $\Delta\Phi$ parameters from Table V are used.

For the determination of the uncertainties of the CPV tests, the following tensor $\langle C^2\rangle_{\mu\nu}$ representing properties of the production process will be needed:

$$\langle C^2\rangle_{\mu\nu} \coloneqq \frac{1}{4\pi}\int \frac{C^2_{\mu\nu}}{C_{00}}\mathrm{d}\Omega_B = \frac{1}{2}\int_{-1}^{1}\frac{C^2_{\mu\nu}}{C_{00}}\mathrm{d}\cos\theta. \quad (41)$$

The production tensor is symmetric and positively defined. In addition, $\langle C^2\rangle_{00} = 1$. For example, it can be used to express the mean-squared polarization $\langle \mathbf{P}_B^2\rangle$ of the B-baryon defined as

$$\langle \mathbf{P}_B^2\rangle = \int \mathbf{P}_B^2\left(\frac{1}{\sigma}\frac{\mathrm{d}\sigma}{\mathrm{d}\Omega_B}\right)\mathrm{d}\Omega_B = \sum_{i=1}^{3}\langle C^2_{i0}\rangle. \quad (42)$$

This integral can be calculated exactly, and the result can be expressed as a linear function of the electron polarization squared P_e^2,

$$\langle \mathbf{P}_B^2\rangle = \mathbb{p}_0 + \mathbb{p}_2 P_e^2, \quad (43)$$

where the expressions for coefficients $\mathbb{p}_0$ and $\mathbb{p}_2$ are given in Appendix D. As we will show later, $\langle \mathbf{P}_B^2\rangle$ determines the uncertainty of the A_{CP} and Φ_{CP} measurement. The results for $\sqrt{\langle \mathbf{P}_B^2\rangle}$ are shown in Fig. 4. We will use the following notation for the polarization and spin-correlation contributions of the production-process tensor:

$$\langle \mathbb{P}_B^2\rangle \coloneqq \sum_{i=1}^{3}(\langle C^2\rangle_{i0} + \langle C^2\rangle_{0i}) = 2\langle \mathbf{P}_B^2\rangle$$
$$\langle \mathbb{S}^2_{B\bar{B}}\rangle = \sum_{i,j=1}^{3}\langle C^2\rangle_{ij}. \quad (44)$$

The values of the $\langle \mathbb{P}_B^2\rangle$ and $\langle \mathbb{S}^2_{B\bar{B}}\rangle$ terms as function of P_e are shown in Fig. 5 for some processes which are discussed later. The dependence on the P_e is much stronger for the polarization terms than for the spin-correlation terms. As we will show in Secs. IV and V, the sizes of the

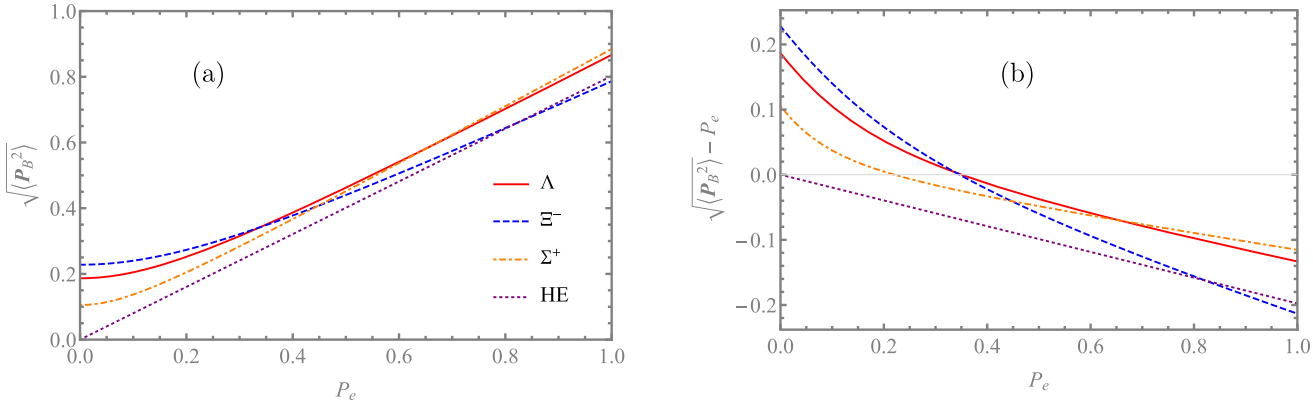

FIG. 4. Average polarization $\sqrt{\langle \mathbf{P}_B^2\rangle}$ for Λ (solid line), Ξ^- (dashed line), Σ^+ (dot-dashed line), and high-energy limit (dotted line) as a function of electron beam polarization is shown in panel (a). In panel (b), the quantity $\sqrt{\langle \mathbf{P}_B^2\rangle} - P_e$ is plotted to facilitate a more precise comparison. The low-energy limit corresponds to $P_B = P_e$.

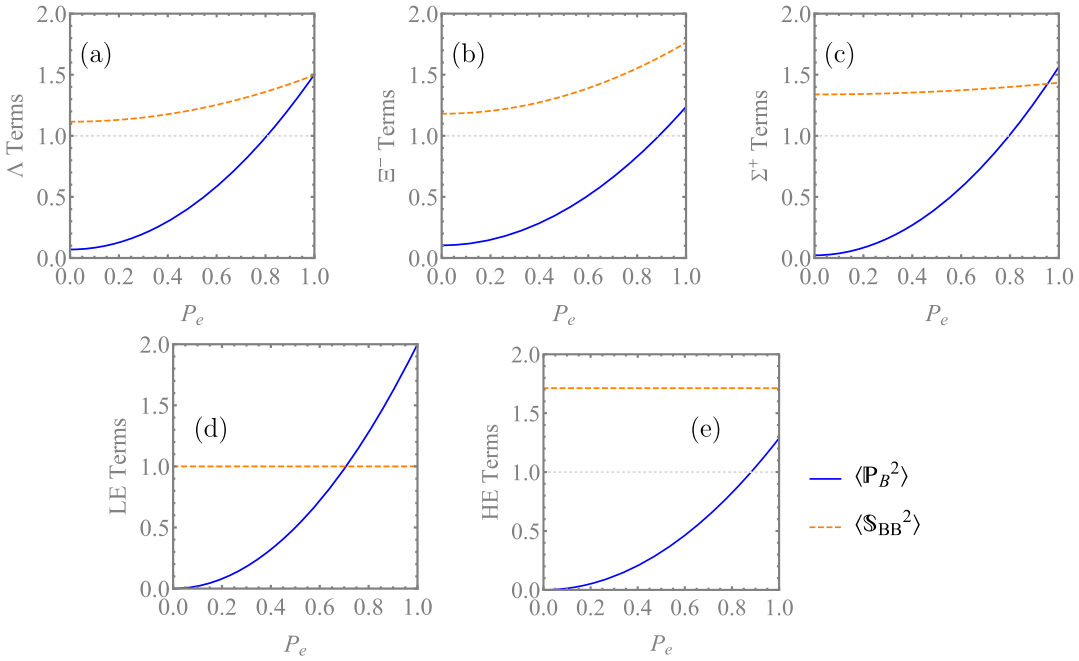

FIG. 5. Polarization $\langle \mathbb{P}_B^2 \rangle$ (solid lines) and spin-correlation terms $\langle \mathbb{S}_{B\bar{B}}^2 \rangle$ (dashed lines) of the $e^+e^- \to B\bar{B}$ processes: (a) $J/\psi \to \Lambda\bar{\Lambda}$, (b) $J/\psi \to \Xi\bar{\Xi}$, (c) $J/\psi \to \Sigma\bar{\Sigma}$, (d) low-energy limit, and (e) high-energy limit.

contributions determine the precision of the CPV observables.

B. Joint angular distributions

The complete joint angular distributions for a production process $e^+e^- \to B\bar{B}$ followed by weak two-body decays of the hyperon B and the antihyperon $\bar{B}$ can be obtained using the modular framework from Ref. [45]. For a single-step decay $D(B \to b\pi)$ and the corresponding c.c. decay mode $\bar{D}(\bar{B} \to \bar{b}\,\bar{\pi})$, like $e^+e^- \to J/\psi \to \Lambda\bar{\Lambda}$ with $\Lambda \to p\pi^-$ and $\bar{\Lambda} \to \bar{p}\pi^+$, the joint angular distribution,

$$\mathcal{P}^{D\bar{D}}(\boldsymbol{\xi};\boldsymbol{\omega}) := \frac{1}{\Gamma}\frac{\mathrm{d}\Gamma}{\mathrm{d}\boldsymbol{\xi}}, \tag{45}$$

is

$$\mathcal{P}^{D\bar{D}}(\boldsymbol{\xi};\boldsymbol{\omega}) = \frac{1}{(4\pi)^3}\sum_{\mu,\nu=0}^{3} C_{\mu\nu}(\Omega_B;\alpha_\psi,\Delta\Phi,P_e)\,a^D_{\mu 0}(\Omega_b;\alpha_D)\,a^{\bar{D}}_{\nu 0}(\Omega_{\bar{b}};\bar{\alpha}_D). \tag{46}$$

There are five global parameters to describe the complete angular distribution, and they are represented by the vector $\boldsymbol{\omega} := (\alpha_\psi, \Delta\Phi, P_e, \alpha_D, \bar{\alpha}_D)$. The vector $\boldsymbol{\xi} := (\Omega_B, \Omega_b, \Omega_{\bar{b}})$ represents a complete set of the kinematic variables describing a single-event configuration in the six-dimensional phase space.

We use *helicity angles* to parametrize the multidimensional phase space. These are spherical coordinates in the *helicity reference frames* of the baryons, defined as follows. In the B baryon rest frame with the z axis defined by the unit vector $\hat{\mathbf{z}}_B$, the direction of the b baryon momentum is denoted as $\hat{\mathbf{p}}_b$. The b-baryon helicity system is the b rest frame where the orientation of the Cartesian coordinate system is given by the unit vectors:

$$\hat{\mathbf{x}}_b = \frac{\hat{\mathbf{z}}_B \times \hat{\mathbf{p}}_b}{|\hat{\mathbf{z}}_B \times \hat{\mathbf{p}}_b|} \times \hat{\mathbf{p}}_b, \quad \hat{\mathbf{y}}_b = \frac{\hat{\mathbf{z}}_B \times \hat{\mathbf{p}}_b}{|\hat{\mathbf{z}}_B \times \hat{\mathbf{p}}_b|} \quad \text{and} \quad \hat{\mathbf{z}}_b = \hat{\mathbf{p}}_b. \tag{47}$$

The production is described by the spin-correlation matrix $C_{\mu\nu}(\Omega_B;\alpha_\psi,\Delta\Phi,P_e)$ in Eq. (37) and the 4×4 decay matrices $a^D_{\mu 0} := a^D_{\mu 0}(\Omega_b;\alpha_D)$ and $a^{\bar{D}}_{\nu 0} := a^{\bar{D}}_{\nu 0}(\Omega_{\bar{b}};\bar{\alpha}_D)$. The decay matrices $a^D_{\mu\nu}$ represent the transformations of the spin operators (Pauli matrices) σ^B_μ and σ^b_ν defined in the B and b baryon helicity frames, respectively [45]:

$$\sigma^B_\mu \to \sum_{\nu=0}^{3} a^D_{\mu\nu}\sigma^b_\nu. \tag{48}$$

The explicit form of the $a^D_{\mu\nu}(\Omega;\alpha_D,\beta_D,\gamma_D) \leftrightarrow a^D_{\mu\nu}(\{\theta,\varphi\};\alpha_D,\beta_D,\gamma_D)$ matrix, representing the polarization vector transformation from Eq. (7) in our framework, is

$$\begin{pmatrix} 1 & 0 & 0 & \alpha_D \\ \alpha_D \sin\theta\cos\varphi & \gamma_D\cos\theta\cos\varphi - \beta_D\sin\varphi & -\beta_D\cos\theta\cos\varphi - \gamma_D\sin\varphi & \sin\theta\cos\varphi \\ \alpha_D \sin\theta\sin\varphi & \beta_D\cos\varphi + \gamma_D\cos\theta\sin\varphi & \gamma_D\cos\varphi - \beta_D\cos\theta\sin\varphi & \sin\theta\sin\varphi \\ \alpha_D\cos\theta & -\gamma_D\sin\theta & \beta_D\sin\theta & \cos\theta \end{pmatrix}. \tag{49}$$

For the single-step processes, only the first column $a_{\mu 0}(\Omega;\alpha_D)$ is used, and it depends only on the decay parameter α_D.

For the processes with two-step decays like $e^+e^- \to \Xi\bar{\Xi}$ with $\Xi \to \Lambda\pi$, $\Lambda \to p\pi^-+$ c.c., the joint angular distribution reads

$$\mathcal{P}^{\Xi\bar{\Xi}}(\boldsymbol{\xi}_{\Xi\bar{\Xi}};\boldsymbol{\omega}_\Xi) = \frac{1}{(4\pi)^5}\sum_{\mu,\nu=0}^{3} C_{\mu\nu}\left(\sum_{\mu'=0}^{3} a^{\Xi}_{\mu\mu'}a^{\Lambda}_{\mu'0}\right)\left(\sum_{\nu'=0}^{3} a^{\bar{\Xi}}_{\nu\nu'}a^{\bar{\Lambda}}_{\nu'0}\right), \tag{50}$$

where $\boldsymbol{\xi}_{\Xi\bar{\Xi}} \coloneqq (\Omega_\Xi, \Omega_\Lambda, \Omega_{\bar{\Lambda}}, \Omega_p, \Omega_{\bar{p}})$ and $\boldsymbol{\omega}_\Xi \coloneqq (\alpha_\psi, \Delta\Phi, P_e, \alpha_\Xi, \bar{\alpha}_\Xi, \phi_\Xi, \bar{\phi}_\Xi, \alpha_\Lambda, \bar{\alpha}_\Lambda)$—the phase space has ten dimensions, and there are nine global parameters.

The ST distributions are obtained by integrating out the unmeasured variables. For example, the ST angular distribution of the B baryon measurement for single sequence decays Eq. (46) is

$$\begin{aligned}\mathcal{P}^D(\boldsymbol{\xi}_b;\boldsymbol{\omega}) &= \frac{1}{(4\pi)^2}\sum_{\mu=0}^{3} C_{\mu 0}\cdot a^D_{\mu 0} \\ &= \frac{1}{(4\pi)^2} C_{00}\cdot(1+\alpha_D \mathbf{P}_B\cdot\hat{\mathbf{p}}_b),\end{aligned} \tag{51}$$

where $\boldsymbol{\xi}_B \coloneqq (\Omega_B, \Omega_b)$ and $\mathbf{P}_B$ is given by Eq. (40). For the reference for comparing the ST uncertainties to the DT measurements with N reconstructed events, we will use a set of two independent ST experiments where the baryon and antibaryon decays are analyzed with N reconstructed events each.

C. Asymptotic maximum likelihood method

The importance of the individual parameters ω_k in the joint angular probability density functions (PDFs) of Eqs. (46) and (50) and their correlations are studied using an ideal asymptotic maximum likelihood method, discussed in Ref. [46]. The method allows one to reliably estimate the statistical accuracy of the determined global parameters in experiments with large acceptance detectors.

The asymptotic expression of the inverse covariance matrix element kl between parameters ω_k and ω_l of the parameter vector $\boldsymbol{\omega}$ is given by the Fisher information matrix [84],

$$\mathcal{I}(\omega_k,\omega_l) \coloneqq N\int \frac{1}{\mathcal{P}}\frac{\partial\mathcal{P}}{\partial\omega_k}\frac{\partial\mathcal{P}}{\partial\omega_l}\mathrm{d}\boldsymbol{\xi}, \tag{52}$$

where N is the number of events in the final selection.[2] The calculated values are used to construct the matrix, which is inverted to obtain the covariance matrix $V = \mathcal{I}^{-1}$ for the parameters. Since asymptotically, in the case of negligible background, the statistical uncertainties given by the standard deviations (SDs), $\sigma(\omega_k)$, are inversely proportional to the square root of the number of the reconstructed signal events N, we will use the product

$$\sigma_C(\omega_k) \coloneqq \sigma(\omega_k)\times\sqrt{N}, \tag{53}$$

and call it *SD coefficient* or normalized statistical uncertainty. It allows for a comparison of the precision of different estimators for a given number of reconstructed events. In most cases, the integral Eq. (52) has to be calculated numerically. However, in this approach, the explicit dependence on the production and decay parameters is hidden, and the calculations have to be repeated for each parameter set. Therefore, we have constructed analytic approximations, which are presented and discussed in the two following sections.

IV. SINGLE-STEP DECAYS

We derive an approximate analytic solution for standard deviation of the A_{CP} measured in a single-step processes described by the PDF in Eq. (46). The straightforward method is to determine all elements of the 5×5 inverse covariance matrix corresponding to the parameter vector $\boldsymbol{\omega} = (\alpha_\psi, \Delta\Phi, P_e, \alpha_D, \bar{\alpha}_D)$, invert the matrix, and use error

[2]In Appendix E, we show how our results should be modified when there is a significant fraction of background events.

propagation to determine the variance $\mathrm{Var}(A_{\mathrm{CP}})$. If the parameter vector can be changed to include the A_{CP} observable and to have the remaining parameters uncorrelated, then the variance $\mathrm{Var}(A_{\mathrm{CP}})$ will be simply given as the inverse of the corresponding information matrix element

$$\frac{1}{\mathrm{Var}(A_{\mathrm{CP}})} = \mathcal{I}(A_{\mathrm{CP}}) \coloneqq N \int \frac{1}{\mathcal{P}^{D\bar{D}}} \left(\frac{\partial \mathcal{P}^{D\bar{D}}}{\partial A_{\mathrm{CP}}}\right)^2 \mathrm{d}\boldsymbol{\xi}. \quad (54)$$

Such parametrization can be constructed using the $\langle \alpha_D \rangle$ and A_{CP} parameters and expressing $\alpha_D = \langle \alpha_D \rangle (1 + A_{\mathrm{CP}})$ and $\bar{\alpha}_D = -\langle \alpha_D \rangle (1 - A_{\mathrm{CP}})$. The new parameter set leads to the expression for the partial derivative of $\mathcal{P}^{D\bar{D}}$ with respect to A_{CP} (taken at $A_{\mathrm{CP}} = 0$),

$$\frac{\partial \mathcal{P}^{D\bar{D}}}{\partial A_{\mathrm{CP}}} = \frac{\langle \alpha_D \rangle}{\mathcal{V}} \sum_{\mu,\nu=0}^{3} C_{\mu\nu} \left(\frac{\partial a^D_{\mu 0}}{\partial \alpha_D} a^{\bar{D}}_{\nu 0} + a^D_{\mu 0} \frac{\partial a^{\bar{D}}_{\nu 0}}{\partial \bar{\alpha}_D} \right) \quad (55)$$

$$= \frac{\alpha_D}{\mathcal{V}} C_{00} (\mathbf{P}_B \cdot \hat{\mathbf{p}}_b - \mathbf{P}_{\bar{B}} \cdot \hat{\mathbf{p}}_{\bar{b}}), \quad (56)$$

where $\mathcal{V} \coloneqq \int \mathrm{d}\boldsymbol{\xi} = \int \mathrm{d}\Omega_B \mathrm{d}\Omega_b \mathrm{d}\Omega_{\bar{b}} = (4\pi)^3$ and $\langle \alpha_D \rangle = \alpha_D$ in the $A_{\mathrm{CP}} = 0$ limit. To calculate the information $\mathcal{I}(A_{\mathrm{CP}})$, we will use the representation for the $\mathcal{P}$ PDF,

$$\mathcal{P}(\boldsymbol{\xi}; \boldsymbol{\omega}) \coloneqq C_{00} \frac{1 + \mathcal{G}(\boldsymbol{\xi}; \boldsymbol{\omega})}{\mathcal{V}}, \quad (57)$$

where $\int \mathcal{G} \mathrm{d}\boldsymbol{\xi} = 0$ and $\mathcal{G} \geq -1$. In addition, all terms included in the function $\mathcal{G}$ are multiplied by $\pm\alpha_D$, and for small values of $|\alpha_D|$ are suppressed. Therefore, it is not unreasonable to use the expansion of $1/(1 + \mathcal{G})$ to approximate $1/\mathcal{P}$:

$$\frac{1}{\mathcal{P}} = \frac{\mathcal{V}}{C_{00}} \frac{1}{1 + \mathcal{G}} = \frac{\mathcal{V}}{C_{00}} \sum_{i=0}^{\infty} (-\mathcal{G})^i \quad (58)$$

and

$$\mathcal{I}(\omega_k, \omega_l) \coloneqq \mathcal{I}_0(\omega_k, \omega_l) + \sum_{i=1}^{\infty} (-1)^i \Delta\mathcal{I}_i(\omega_k, \omega_l) \quad (59)$$

with

$$\mathcal{I}_0(\omega_k, \omega_l) \coloneqq N \int \frac{\mathcal{V}}{C_{00}} \frac{\partial \mathcal{P}}{\partial \omega_k} \frac{\partial \mathcal{P}}{\partial \omega_l} \mathrm{d}\boldsymbol{\xi}, \quad (60)$$

$$\Delta\mathcal{I}_i(\omega_k, \omega_l) \coloneqq N \int \frac{\mathcal{V}}{C_{00}} \mathcal{G}^i \frac{\partial \mathcal{P}}{\partial \omega_k} \frac{\partial \mathcal{P}}{\partial \omega_l} \mathrm{d}\boldsymbol{\xi}. \quad (61)$$

We can always compare this analytic result using one or more terms of the expansion with the full numerical calculations. The hope is that the analytic approximation reproduces main features of the exact solution. If it does, it will facilitate understanding how the uncertainties depend on the global parameters. We start by considering the 0th term of the above expansion, $\mathcal{V}/C_{00}$, that leads to the following information:

$$\mathcal{I}_0(A_{\mathrm{CP}}) = N \int \frac{\mathcal{V}}{C_{00}} \left(\frac{\partial \mathcal{P}^{D\bar{D}}}{\partial A_{\mathrm{CP}}}\right)^2 \mathrm{d}\Omega_B \mathrm{d}\Omega_b \mathrm{d}\Omega_{\bar{b}} \quad (62)$$

$$= N \frac{\alpha_D^2}{\mathcal{V}} \int C_{00} (\mathbf{P}_B \cdot \hat{\mathbf{p}}_b - \mathbf{P}_{\bar{B}} \cdot \hat{\mathbf{p}}_{\bar{b}})^2 \mathrm{d}\Omega_B \mathrm{d}\Omega_b \mathrm{d}\Omega_{\bar{b}}. \quad (63)$$

Integration over Ω_b and $\Omega_{\bar{b}}$ simplifies due to orthonormality:

$$\begin{aligned} &\int (\mathbf{P}_B \cdot \hat{\mathbf{p}}_b - \mathbf{P}_{\bar{B}} \cdot \hat{\mathbf{p}}_{\bar{b}})^2 \frac{\mathrm{d}\Omega_b}{4\pi} \frac{\mathrm{d}\Omega_{\bar{b}}}{4\pi} \\ &= \int (\mathbf{P}_B \cdot \hat{\mathbf{p}}_b)^2 \frac{\mathrm{d}\Omega_b}{4\pi} + \int (\mathbf{P}_{\bar{B}} \cdot \hat{\mathbf{p}}_{\bar{b}})^2 \frac{\mathrm{d}\Omega_{\bar{b}}}{4\pi} \\ &= \frac{\mathbf{P}_B^2}{3} + \frac{\mathbf{P}_{\bar{B}}^2}{3} = \frac{2}{3} \mathbf{P}_B^2. \end{aligned}$$

Inserting the result into Eq. (56) and Eq. (62), we have

$$\begin{aligned} \mathcal{I}_0(A_{\mathrm{CP}}) &= \frac{N}{4\pi} \alpha_D^2 \frac{2}{3} \int \mathbf{P}_B^2 C_{00} \mathrm{d}\Omega_B \\ &= \frac{2N}{3} \alpha_D^2 \int \mathbf{P}_B^2 \left(\frac{1}{\sigma} \frac{\mathrm{d}\sigma}{\mathrm{d}\Omega_B}\right) \mathrm{d}\Omega_B = \frac{2N}{3} \alpha_D^2 \langle \mathbf{P}_B^2 \rangle. \end{aligned} \quad (64)$$

Therefore, in this approximation, the information is proportional to the B-baryon average squared polarization, as defined in Eq. (42). Since A_{CP} is not correlated with other variables, the 0th approximation for the uncertainty is

$$\sigma(A_{\mathrm{CP}}) \sqrt{N} = \sigma_C(A_{\mathrm{CP}}) \approx \sqrt{\frac{3}{2}} \frac{1}{\alpha_D \sqrt{\langle \mathbf{P}_B^2 \rangle}}. \quad (65)$$

Figure 6(a) shows the SD coefficients, $\sigma_C(A_{\mathrm{CP}}^{[\Lambda p]})$, multiplied by the α_Λ parameter value for the $e^+e^- \to J/\psi \to \Lambda\bar{\Lambda}$ processes. The 0th-order result (hereafter, we will call it also the analytic approximation) is close to the numerical full result in Eq. (52), even if α_Λ is relatively large (0.75). This shows that the influence of the higher-order terms is low for the $A_{\mathrm{CP}}^{[\Lambda p]}$ determination.

We also compare the approximate analytic formula to the full numerical calculations for the $e^+e^- \to J/\psi \to \Sigma^+\bar{\Sigma}^-$ process, where both α_ψ and $\Delta\Phi$ have been measured by BESIII [54]. The two Σ^+ decay modes $\Sigma n(\Sigma^+ \to n\pi^+)$ and $\Sigma p(\Sigma^+ \to p\pi^0)$ are interesting as the limiting cases for the expansion since $\alpha_{\Sigma n} = 0.068 \approx 0$ and $\alpha_{\Sigma p} = -0.994 \approx -1$, respectively. It is worth noting that in the $\Delta I = 1/2$ limit $|\alpha_{\Sigma p}| < \cos(\delta_1^P - \delta_1^S) \approx 0.980$ [see Eq. (23) and the values of the strong phase shifts in Table III]. We note that the recent BESIII value $\langle \alpha_{\Sigma p} \rangle = -0.994(4)$ (Table II) violates

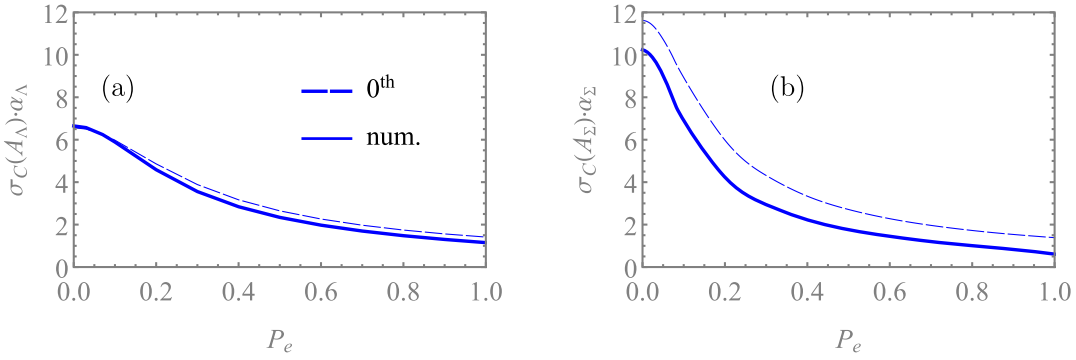

FIG. 6. Standard deviation coefficients for $A_{\rm CP}$, $\sigma_C(A_{\rm CP})$, multiplied by the decay parameter value α_D for DT measurements. (a) $e^+e^- \to J/\psi \to \Lambda\bar{\Lambda}$ with decay $\Lambda(\Lambda \to p\pi^-)$. (b) $e^+e^- \to J/\psi \to \Sigma^+\bar{\Sigma}^-$ with decay $\Sigma p(\Sigma^+ \to p\pi^0)$. Dashed lines are the approximations using Eq. (65), and solid lines are the exact numerical results.

this bound. A proper interpretation of this result requires that all isospin contributions to the Σ^+ decays are considered, but such discussion is beyond the scope of this report. The 0th approximation for $\sigma_C(A_{\rm CP}^{\Sigma p}) \cdot |\alpha_{\Sigma p}|$ is given by the dashed line in Fig. 6(b). The full numerical result (given by the solid line) differs significantly. The difference comes from the spin-correlation contributions, but the analytic approximation is able to describe the overall trend. From Eq. (65), it is clear that the approximation for $\sigma_C(A_{\rm CP}^{\Sigma n})\alpha_{\Sigma n}$ is also given by the same dashed line. As expected, the full numerical result coincides with the 0th approximation in this case. Comparing the trends for Λ and Σ^+, the faster decrease of the uncertainty for Σ^+ is mainly due to the low value of the $\Delta\Phi$ phase for this reaction. In principle, this would make Σp an attractive decay mode for testing *CP* symmetry with a polarized electron beam. However, we will not discuss further the Σ-baryon decays in this report. The reason is that the predicted CPV effects are significantly smaller, $A_{\rm CP}^{\Sigma p} \cdot \alpha_{\Sigma p} \approx 3.5 \times 10^{-6}$ and $A_{\rm CP}^{\Sigma n} \cdot \alpha_{\Sigma n} \approx 2.7 \times 10^{-5}$ [26], and the isospin structure of the amplitudes is more complicated (since also $\Delta I = 5/2$ transitions contribute).

The result for $\sigma_C(A_{\rm CP}^D)$ in the DT and ST cases is the same when the ST analysis is done under assumption that the $\langle\alpha_D\rangle$ value is known and fixed. In a single-step decay, an ST measurement only allows for a determination of the products $\alpha_D\sqrt{\langle P_B^2\rangle}$ and $\bar{\alpha}_D\sqrt{\langle P_{\bar{B}}^2\rangle}$. Therefore, a $A_{\rm CP}^D$ determination using a combination of baryon-antibaryon ST measurements requires knowledge of the polarization through some other means or using a production process where $\langle P_B^2\rangle = \langle P_{\bar{B}}^2\rangle$ is assured. For an $e^+e^- \to B\bar{B}$ experiment with an electron beam polarization P_e where the ST data are collected simultaneously and with c.c. symmetric detector acceptance, this condition is fulfilled automatically.

Related to this discussion is a proposal given in Ref. [85], in which it is suggested that one could use a triple vector product to determine $A_{\rm CP}$ even if $\Delta\Phi = 0$ and $P_e = 0$, i.e., the baryons are unpolarized. For a general baryon-antibaryon state with polarization terms set to zero, the angular distribution after single-step decays reads

$$\mathcal{P}^{D\bar{D}} \propto C_{00} + \alpha_D\bar{\alpha}_D \sum_{i,j=1}^{3} C_{ij}\left[\frac{a_{i0}^D}{\alpha_D}\right]\left[\frac{a_{j0}^{\bar{D}}}{\bar{\alpha}_D}\right] =: C_{00} + \alpha_D\bar{\alpha}_D\mathcal{F}(\Omega_B, \Omega_b, \Omega_{\bar{b}}), \tag{66}$$

where $\mathcal{F}(\ldots)$ is a function of the kinematic variables only. Therefore, the PDF is described by a single global parameter $\alpha_{D\bar{D}} := \alpha_D\bar{\alpha}_D = -\langle\alpha_D\rangle^2(1 - A_{\rm CP}^2)$. The parameter is related to $A_{\rm CP}$ and can in principle be used to test *CP* symmetry, but the method has several drawbacks. The information for $\alpha_{D\bar{D}}$ measurement is $\mathcal{I}_0(\alpha_{D\bar{D}}) = N/9\langle\mathbb{S}^2\rangle$, and the uncertainty of $A_{\rm CP}$ from the error propagation is

$$\sigma(A_{\rm CP}) = \frac{1}{A_{\rm CP}}\sqrt{\sigma^2(\langle\alpha_D\rangle) + \frac{\sigma^2(\alpha_{D\bar{D}})}{4\langle\alpha_D\rangle^2}},$$

which requires an independent determination of $\langle\alpha_D\rangle$. A meaningful *CP* test is possible only if $\sigma(A_{\rm CP}) < 1$. This requires that the $\sigma(\langle\alpha_D\rangle)$ precision is better than $\mathcal{O}(10^{-5})$, since $A_{\rm CP} \sim \mathcal{O}(10^{-5})$ in the SM. If $\sigma(\langle\alpha_D\rangle)$ is not small enough, the $A_{\rm CP} \neq 0$ value can be interpreted as a $A_{\rm CP}$ null result but with the decay parameters α_D and $\bar{\alpha}_D$ reduced by the factor $\sqrt{1 - A_{\rm CP}^2}$.

V. TWO-STEP DECAYS

To study uncertainties of the *CP* asymmetries in $e^+e^- \to \Xi^-\bar{\Xi}^+$, we rewrite Eq. (50) as

$$\mathcal{P}^{\Xi\bar{\Xi}}(\boldsymbol{\xi}_{\Xi\bar{\Xi}}; \boldsymbol{\omega}_\Xi) = \frac{1}{\mathcal{V}}\sum_{\mu,\nu=0}^{3} C_{\mu\nu}\mathcal{D}_\Xi^\mu\bar{\mathcal{D}}_\Xi^\nu \tag{67}$$

using the following notation:

$$\mathcal{D}^{\mu}_{\Xi} \coloneqq \mathcal{D}^{\mu}(\Omega_{\Lambda},\Omega_{p};\alpha_{\Xi},\phi_{\Xi},\alpha_{\Lambda}) \coloneqq \sum_{\mu'=0}^{3} a^{\Xi}_{\mu\mu'} a^{\Lambda}_{\mu'0},$$

$$\bar{\mathcal{D}}^{\mu}_{\Xi} \coloneqq \mathcal{D}^{\mu}(\Omega_{\bar{\Lambda}},\Omega_{\bar{p}};\bar{\alpha}_{\Xi},\bar{\phi}_{\Xi},\bar{\alpha}_{\Lambda}) \coloneqq \sum_{\mu'=0}^{3} a^{\bar{\Xi}}_{\mu\mu'} a^{\bar{\Lambda}}_{\mu'0},$$

$$\mathcal{V} \coloneqq \int \mathrm{d}\boldsymbol{\xi}_{\Xi\bar{\Xi}} = (4\pi)^5.$$

We use a modified parameter set where α_D and $\bar{\alpha}_D$ are expressed by A^{D}_{CP} and $\langle\alpha_D\rangle$. For $A^{[\Xi-]}_{\mathrm{CP}}$ and $A^{[\Lambda p]}_{\mathrm{CP}}$, we use a simplified notation A_{Ξ} and A_{Λ}, respectively. Similarly, we use $\Phi^{[\Xi-]}_{\mathrm{CP}}$ (denoted as Φ_{CP}) to represent $\phi_{\Xi} = \Phi_{\mathrm{CP}} + \langle\phi_{\Xi}\rangle$ and $\bar{\phi}_{\Xi} = \Phi_{\mathrm{CP}} - \langle\phi_{\Xi}\rangle$. The vector of the parameters related to the Ξ and Λ decays is $\boldsymbol{\omega} \coloneqq (\langle\alpha_{\Xi}\rangle, \langle\phi_{\Xi}\rangle, \langle\alpha_{\Lambda}\rangle, A_{\Xi}, \Phi_{\mathrm{CP}}, A_{\Lambda})$. Therefore, the partial derivative, e.g., with respect to Φ_{CP} is

$$\frac{\partial\mathcal{P}^{\Xi\bar{\Xi}}}{\partial\Phi_{\mathrm{CP}}} = \frac{1}{\mathcal{V}}\sum_{\mu,\nu=0}^{3} C_{\mu\nu}\left(\frac{\partial\mathcal{D}^{\mu}_{\Xi}}{\partial\phi_{\Xi}}\bar{\mathcal{D}}^{\nu}_{\Xi} + \mathcal{D}^{\mu}_{\Xi}\frac{\partial\bar{\mathcal{D}}^{\nu}_{\Xi}}{\partial\bar{\phi}_{\Xi}}\right).$$

Because of the orthonormality of the decay and production functions, the information matrix elements related to the decay parameters ω_i and ω_j can be written as

$$\mathcal{I}_0(\omega_i,\omega_j) = N\sum_{\mu,\nu=0}^{3}\langle C^2\rangle_{\mu\nu}\langle\Delta_{\omega_i}\Delta_{\omega_j}\rangle^{\mu\nu}. \tag{68}$$

We have checked these orthonormality relations in the explicit calculations. The production tensor is defined in Eq. (41). The decay tensor is

$$\langle\Delta_{\omega_i}\Delta_{\omega_j}\rangle^{\mu\nu} \coloneqq \frac{1}{(4\pi)^4}\int\frac{\partial(\mathcal{D}^{\mu}_{\Xi}\bar{\mathcal{D}}^{\nu}_{\Xi})}{\partial\omega_i}\frac{\partial(\mathcal{D}^{\mu}_{\Xi}\bar{\mathcal{D}}^{\nu}_{\Xi})}{\partial\omega_j}\mathrm{d}\Omega_{\Lambda}\mathrm{d}\Omega_{p}\mathrm{d}\Omega_{\bar{\Lambda}}\mathrm{d}\Omega_{\bar{p}}. \tag{69}$$

For example, $\mathcal{I}_0(\Phi_{\mathrm{CP}})$ can be expressed as

$$\begin{aligned}\mathcal{I}_0(\Phi_{\mathrm{CP}}) &= N\int\frac{\mathcal{V}}{C_{00}}\left(\frac{\partial\mathcal{P}^{\Xi\bar{\Xi}}}{\partial\Phi_{\mathrm{CP}}}\right)^2\mathrm{d}\boldsymbol{\xi}\\ &= N\sum_{\mu,\nu=0}^{3}\left[\frac{1}{4\pi}\int\frac{C^2_{\mu\nu}}{C_{00}}\mathrm{d}\Omega_{\Xi}\right]\left[\frac{1}{(4\pi)^4}\int\left(\frac{\partial(\mathcal{D}^{\mu}_{\Xi}\bar{\mathcal{D}}^{\nu}_{\Xi})}{\partial\Phi_{\mathrm{CP}}}\right)^2\mathrm{d}\Omega_{\Lambda}\mathrm{d}\Omega_{p}\mathrm{d}\Omega_{\bar{\Lambda}}\mathrm{d}\Omega_{\bar{p}}\right]\\ &\eqqcolon N\sum_{\mu,\nu=0}^{3}\langle C^2\rangle_{\mu\nu}\langle\Delta^2_{\Phi_{\mathrm{CP}}}\rangle^{\mu\nu}.\end{aligned}$$

The information matrix elements for the decay parameters can be obtained as

$$\mathcal{I}_0(\omega_i,\omega_j) = N[\mathbb{a}_{ij} + \mathbb{b}_{ij}\langle\mathbb{P}^2_{\Xi}\rangle + \mathbb{c}_{ij}\langle\mathbb{S}^2_{\Xi\bar{\Xi}}\rangle], \tag{70}$$

where $\langle\mathbb{P}^2_{\Xi}\rangle(=2\langle\mathbf{P}^2_{\Xi}\rangle)$ and $\langle\mathbb{S}^2_{\Xi\bar{\Xi}}\rangle$ are the sums of the $\langle C^2\rangle_{\mu\nu}$-matrix polarization and spin-correlation elements, respectively, defined in Eq. (44) [and shown for few production processes in Fig. 5(b) as the function of electron-beam polarization]. Such representation is possible since the decay tensor elements have only three different values $\mathbb{a}_{ij}$, $\mathbb{b}_{ij}$, and $\mathbb{c}_{ij}$. It turns out that the only nonzero elements of the information matrix involving the *CP*-odd variables for the two-step process are

$$\mathcal{I}_0(\Phi_{\mathrm{CP}}) = \frac{2N}{27}(1-\alpha^2_{\Xi})\alpha^2_{\Lambda}\left[(3+\alpha^2_{\Xi}\alpha^2_{\Lambda})\langle\mathbb{P}^2_{\Xi}\rangle + \frac{2}{3}(\alpha^2_{\Xi}(3-2\alpha^2_{\Lambda}) + 3\alpha^2_{\Lambda})\langle\mathbb{S}^2_{\Xi\bar{\Xi}}\rangle\right], \tag{71}$$

$$\mathcal{I}_0(A_{\Xi}) = \frac{2N}{3}\alpha^2_{\Lambda}\alpha^2_{\Xi}\left[1 + \frac{3(\alpha^4_{\Lambda}+3) - \alpha^2_{\Xi}(3-\alpha^2_{\Lambda})^2}{18(1-\alpha^2_{\Xi})\alpha^2_{\Lambda}}\langle\mathbb{P}^2_{\Xi}\rangle + \frac{\alpha^2_{\Xi}(2\alpha^2_{\Lambda}-3)+9}{27(1-\alpha^2_{\Xi})}\langle\mathbb{S}^2_{\Xi\bar{\Xi}}\rangle\right], \tag{72}$$

$$\mathcal{I}_0(A_{\Lambda}) = \frac{2N}{3}\alpha^2_{\Lambda}\alpha^2_{\Xi}\left[1 + \frac{\alpha^4_{\Xi}-2\alpha^2_{\Xi}+3}{6\alpha^2_{\Xi}}\langle\mathbb{P}^2_{\Xi}\rangle + \frac{1}{9}(3-2\alpha^2_{\Xi})\langle\mathbb{S}^2_{\Xi\bar{\Xi}}\rangle\right], \tag{73}$$

$$\mathcal{I}_0(A_{\Lambda},A_{\Xi}) = \frac{2N}{3}\alpha^2_{\Lambda}\alpha^2_{\Xi}\left[1 - \frac{1}{3}(\langle\mathbb{P}^2_{\Xi}\rangle + \langle\mathbb{S}^2_{\Xi\bar{\Xi}}\rangle)\right]. \tag{74}$$

These information matrix elements allows one to determine SDs and correlations between the CPV observables. The uncertainty for $\Phi_{\rm CP}$ is $\sigma(\Phi_{\rm CP}) = 1/\sqrt{\mathcal{I}(\Phi_{\rm CP})}$, since the variable is uncorrelated with any other variable. The A_Ξ and A_Λ variables are only correlated with each other, and the covariance matrix is obtained by inverting two-dimensional information matrix

$$\begin{pmatrix} \sigma^2(A_\Xi) & \mathrm{Cov}(A_\Lambda, A_\Xi) \\ \mathrm{Cov}(A_\Lambda, A_\Xi) & \sigma^2(A_\Lambda) \end{pmatrix} = \begin{pmatrix} \mathcal{I}(A_\Xi) & \mathcal{I}(A_\Lambda, A_\Xi) \\ \mathcal{I}(A_\Lambda, A_\Xi) & \mathcal{I}(A_\Lambda) \end{pmatrix}^{-1}. \tag{75}$$

The expressions in Eqs. (71)–(74) have some interesting properties which are valid for any two-step process that can be studied by allowing the α_Λ and α_Ξ parameters to vary. We discuss these properties using a generic notation, where the first decay process is $B \to b\pi$ and the baryon b decays in the sequential weak two-body nonleptonic process:

(i) The $\Phi_{\rm CP}$ uncertainty is not correlated with any other variable, and none of the information matrix elements depends on the $\langle\phi_B\rangle$ value. This is because ϕ_B represents the shift in the φ_b azimuthal angle of the b baryon, which is integrated out. A dependence on $\langle\phi_B\rangle$ might appear in experiments where the acceptance in the φ_b variable is limited.

(ii) For $\alpha_b = 0$ only, $\mathcal{I}_0(A_B) = \frac{1}{3}\alpha_B^2\langle\mathbb{P}_B^2\rangle$ is nonzero, and the CPV test is the same as in a single-step decay.

(iii) For $\alpha_B \to 0$, two terms are nonzero $\mathcal{I}_0(\Phi_{\rm CP}) = \frac{2}{27}\alpha_b^2[3\langle\mathbb{P}_B^2\rangle + 2\alpha_b^2\langle\mathbb{S}_{B\bar{B}}^2\rangle]$ and $\mathcal{I}_0(A_b) = \frac{1}{3}\alpha_b^2\langle\mathbb{P}_B^2\rangle$. Therefore, both $\Phi_{\rm CP}$ and A_b can be measured. In particular, because of the nonzero $\mathbb{c}$-type term for $\mathcal{I}_0(\Phi_{\rm CP})$, the polarization of the B baryon is not needed. This is an attractive scenario for CPV tests for any baryon decaying into Λ.

(iv) The term $\mathcal{I}_0(A_B)$ is divergent for $|\alpha_B| \to 1$, indicating that $\sigma(A_B)$ vanish in this limit. This is a consequence of the $\sqrt{1-\alpha_B^2}$ terms in the angular distribution. The validity of such expressions requires that the boundary $|\alpha_B| \le 1$ must be strictly fulfilled and in the $|\alpha_B| \to 1$ limit there is no linear term in the expansion of the α_B parameter (i.e., the linear error is 0). To get a meaningful result, one should use a parametrization which respects this boundary, such as Eq. (23) from Sec. II B. In principle, one can directly investigate the uncertainty of the weak phase difference $\xi_P - \xi_S$. However, as seen from Eq. (26), this will introduce correlation with the $\Phi_{\rm CP}$ observable (due to the term $\sin\phi$). Instead, one can present results for $\Delta\zeta_B := \alpha_B/\sqrt{1-\alpha_B^2}A_B$, which do not introduce such correlation. The information matrix elements are modified due to the Jacobian of the variable transformation to

$$\mathcal{I}_0(\Delta\zeta_B) = \frac{(1-\alpha_B^2)}{\alpha_B^2}\mathcal{I}_0(A_B),$$
$$\mathcal{I}_0(A_b, \Delta\zeta_B) = \frac{\sqrt{1-\alpha_B^2}}{\alpha_B}\mathcal{I}_0(A_b, A_B).$$

We first discuss uncertainties for the production tensors corresponding to the simplest cases. Unpolarized and uncorrelated sources of B and $\bar{B}$ correspond to $\langle C^2\rangle_{\mu\nu} = \mathrm{diag}(1,0,0,0)$. The only nonzero elements of the information matrix are

$$\mathcal{I}_0(A_B) = \mathcal{I}_0(A_b) = \mathcal{I}_0(A_b, A_B) = N\frac{2}{3}\alpha_b^2\alpha_B^2,$$

where we have assumed samples of N events each for the cascade and anticascade decays. Since the information matrix corresponding to the A_Ξ and A_Λ is singular, the asymmetries are fully correlated and cannot be determined separately, but the sum $A_\Xi + A_\Lambda$ can, and the uncertainty is $\sigma_C(A_\Xi + A_\Lambda) = \sqrt{3/2}/(\alpha_\Lambda\alpha_\Xi)$.

As the next example, we consider two independent ST experiments with N events each using polarized cascades and anticascades having the same average polarization $\langle\mathbf{P}_B^2\rangle$. In the 0th approximation, the expressions for the uncertainties depend on the production mechanism only via the average $\langle\mathbf{P}_B^2\rangle$. For example, in the HyperCP-type experiments, where the initial hyperon polarization is considered to be a fixed vector that does not depend on the kinematic variables of the production process, the average reduces to the square of the vector $\sqrt{\langle\mathbf{P}_B^2\rangle} \to |\mathbf{P}_B|$. The Fisher information matrix is the sum of the matrices for the two ST experiments

$$\mathcal{I}_0(\omega_i, \omega_j) = 2N[\mathbb{a}_{ij} + \mathbb{b}_{ij}\langle\mathbf{P}_B^2\rangle], \tag{76}$$

and the elements of the information matrix for the CP-test observables read

$$\begin{aligned}
\mathcal{I}_0(\Phi_{\rm CP}) &= N\frac{4}{27}(1-\alpha_B^2)\alpha_b^2(3+\alpha_B^2\alpha_b^2)\langle\mathbf{P}_B^2\rangle, \\
\mathcal{I}_0(A_B) &= N\frac{4}{3}\alpha_b^2\alpha_B^2\left[1 + \frac{3(\alpha_b^4+3) - \alpha_B^2(3-\alpha_b^2)^2}{18(1-\alpha_B^2)\alpha_b^2}\langle\mathbf{P}_B^2\rangle\right], \\
\mathcal{I}_0(A_b) &= N\frac{4}{3}\alpha_b^2\alpha_B^2\left[1 + \frac{\alpha_B^4 - 2\alpha_B^2 + 3}{6\alpha_B^2}\langle\mathbf{P}_B^2\rangle\right], \\
\mathcal{I}_0(A_b, A_B) &= N\frac{4}{3}\alpha_b^2\alpha_B^2\left[1 - \frac{1}{3}\langle\mathbf{P}_B^2\rangle\right].
\end{aligned} \tag{77}$$

For two HyperCP-type experiments with $|\mathbf{P}_B| = |\mathbf{P}_{\bar{B}}|$ and N events, each of the formulas are the same. The resulting uncertainties $\sigma_C = \sigma\sqrt{N}$ for the A_Λ, A_Ξ and $A_\Lambda + A_\Xi$ observables measured using the $\Xi^-/\bar{\Xi}^+$ decay chains are shown in Fig. 7(a), while for $\Phi_{\rm CP}$, they are shown in Fig. 7(b).

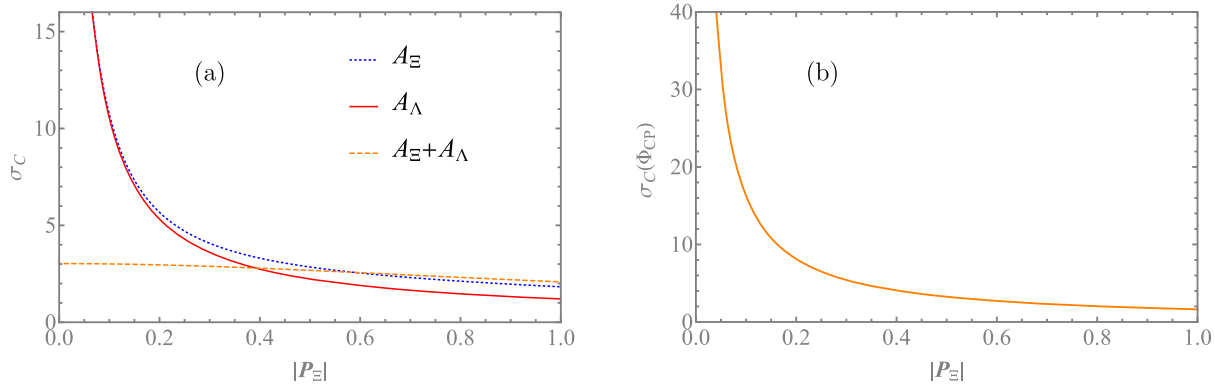

FIG. 7. Uncertainties, σ_C, for CP tests in HyperCP-type experiment using analytic approximation: (a) A_Λ (solid line), A_Ξ (dotted line), and $A_\Lambda + A_\Xi$ (dashed line) and (b) $\Phi_{\rm CP}$.

The uncertainty of the sum $A_\Lambda + A_\Xi$ is nearly independent of the average polarization. Because of the large correlation term $\mathcal{I}(A_\Lambda, A_\Xi)$ in Eq. (77), the relation between the information and uncertainties is not straightforward. However, the 2×2 information matrix for A_Λ and A_Ξ can be diagonalized. The new uncorrelated variables $A_\pm$ are

$$A_\pm \coloneqq \frac{1}{\sqrt{2}}\left[\sqrt[4]{\frac{\mathcal{I}(A_\Lambda)}{\mathcal{I}(A_\Xi)}}A_\Xi \pm \sqrt[4]{\frac{\mathcal{I}(A_\Xi)}{\mathcal{I}(A_\Lambda)}}A_\Lambda\right], \tag{78}$$

where we have chosen an orthonormal transformation. If the polarization $|\mathbf{P}_\Xi|$ is zero, $A_+ = (A_\Lambda + A_\Xi)/\sqrt{2}$ is the only CP-violating variable that can be measured. Since the definition of the variables $A_\pm$ depends on the polarization (and on detection efficiencies in an experiment), we will not use or discuss them further. Since only two weak phases $\Delta\xi^\Xi \coloneqq (\xi_P - \xi_S)^{[\Xi-]}$ and $\Delta\xi^\Lambda \coloneqq (\xi_P - \xi_S)^{[\Lambda p]}$ describe CP violation in the $[\Xi-]$ and $[\Lambda p]$ decays, we provide the corresponding 2×2 Fisher information matrix, which is based on Eq. (52) and does not require the analytic approximation:

$$\begin{aligned}
\mathcal{I}(\Delta\xi^\Xi) &= \mathcal{I}(\Phi_{\rm CP})\frac{1-\langle\alpha_\Xi\rangle^2}{\langle\alpha_\Xi\rangle^2}\cos^2\langle\phi_\Xi\rangle \\
&\quad + \mathcal{I}(A_\Xi)\frac{\langle\alpha_\Xi\rangle^2}{1-\langle\alpha_\Xi\rangle^2}\sin^2\langle\phi_\Xi\rangle, \\
\mathcal{I}(\Delta\xi^\Lambda) &= \mathcal{I}(A_\Lambda)\frac{\langle\alpha_\Lambda\rangle^2}{1-\langle\alpha_\Lambda\rangle^2}\sin^2\langle\phi_\Lambda\rangle, \\
\mathcal{I}(\Delta\xi^\Lambda, \Delta\xi^\Xi) &= \frac{\langle\alpha_\Xi\rangle}{\sqrt{1-\langle\alpha_\Xi\rangle^2}}\sin\langle\phi_\Xi\rangle\frac{\langle\alpha_\Lambda\rangle}{\sqrt{1-\langle\alpha_\Lambda\rangle^2}} \\
&\quad \times \sin\langle\phi_\Lambda\rangle\mathcal{I}(A_\Lambda, A_\Xi).
\end{aligned} \tag{79}$$

However, since $\langle\phi_\Xi\rangle \approx 0$, the $\Phi_{\rm CP}$ measurement gives the dominating contribution to the $\Delta\xi^\Xi$ uncertainty.

Our next case is the decay of a (pseudo)scalar meson like η_c or χ_{c0} into a $B\bar{B}$ pair with the production tensor $\langle C^2\rangle_{\mu\nu} = \mathrm{diag}(1,1,1,1)$. There are no polarization terms, $\langle\mathbb{P}_B^2\rangle = 0$, and $\langle\mathbb{S}_{B\bar{B}}^2\rangle = 3$. The information matrix element $\mathcal{I}_0(A_b, A_B)$ is zero, which means that all three CPV observables are uncorrelated. The diagonal terms of the information matrix are functions of α_b and α_B only:

$$\begin{aligned}
\mathcal{I}_0(\Phi_{\rm CP}) &= N\frac{4}{27}(1-\alpha_B^2)\alpha_b^2[\alpha_B^2(3-2\alpha_b^2)+3\alpha_b^2], \\
\mathcal{I}_0(A_B) &= N\frac{2}{3}\alpha_b^2\alpha_B^2\left[1+\frac{\alpha_B^2(2\alpha_b^2-3)+9}{9(1-\alpha_B^2)}\right], \\
\mathcal{I}_0(A_b) &= N\frac{2}{3}\alpha_b^2\alpha_B^2\left[1+\frac{1}{3}(3-2\alpha_B^2)\right].
\end{aligned}$$

Figure 8 shows the uncertainties σ_C for this case as a function of α_B and α_b decay parameters. This case is

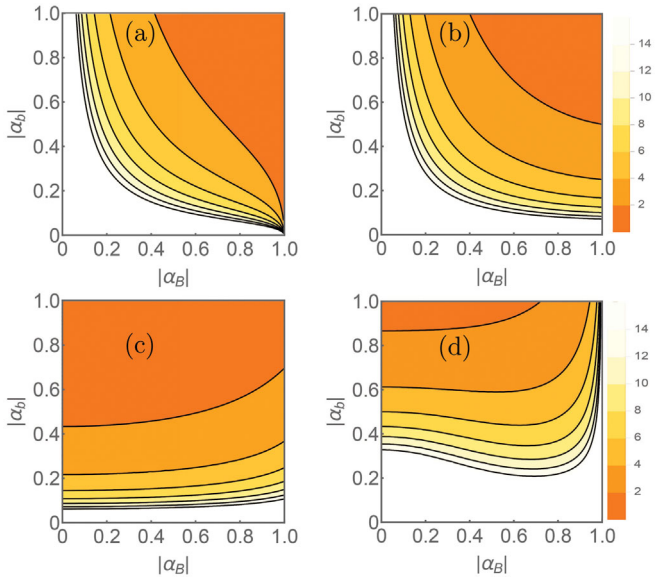

FIG. 8. Statistical uncertainties σ_C of (a) A_B, (b) A_b, (c) $\Delta\zeta_B$, and (d) $\Phi_{\rm CP}$ measurement in a (pseudo)scalar meson decay to $B\bar{B}$ as a function of α_B and α_b treated as free parameters. The white regions in the bottom of the plots correspond to the uncertainties $\sigma_C(\ldots) > 15$.

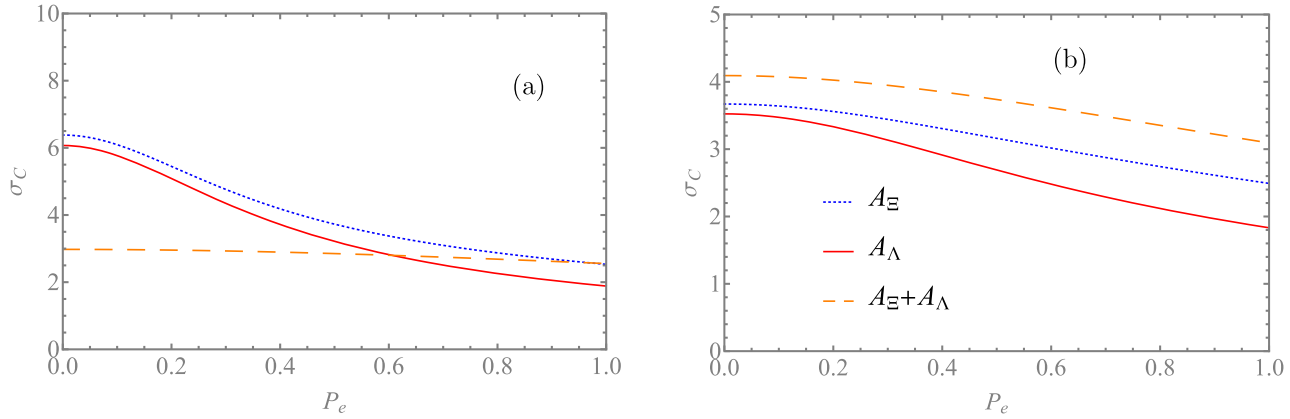

FIG. 9. Uncertainties, σ_C, for the $e^+e^- \to J/\psi \to \Xi\bar{\Xi}$. (a) two ST and (b) DT experiments with N events each: A_Λ (solid line), A_Ξ (dotted line) and $A_\Lambda + A_\Xi$ (dashed line).

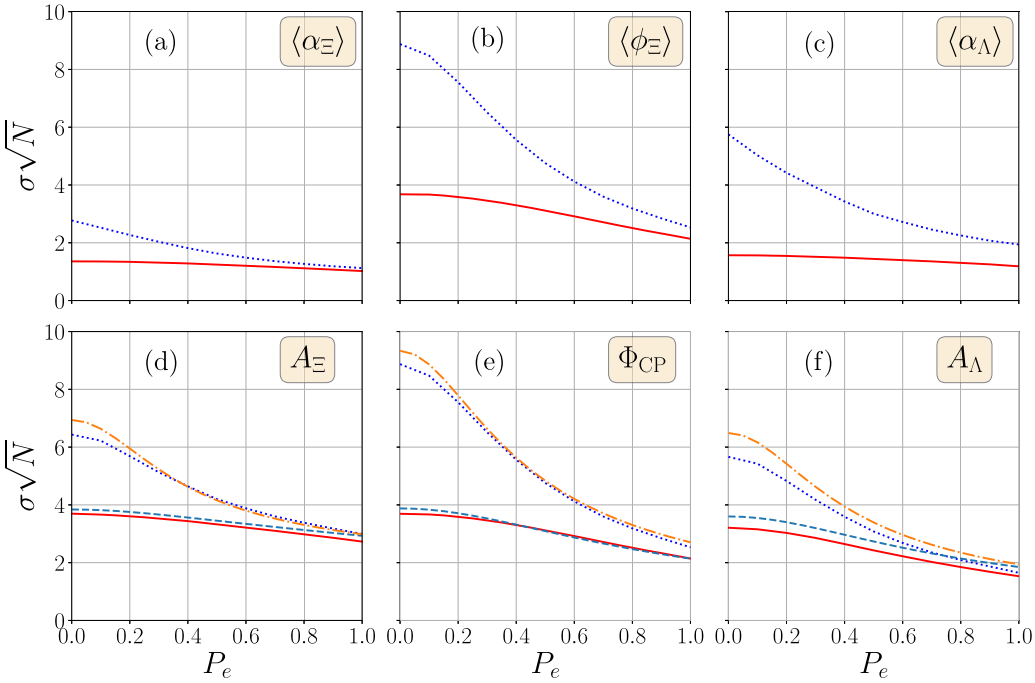

FIG. 10. Numerical estimate of the uncertainty $\sigma\sqrt{N}$ of (a)–(c) average decay parameters and (d)–(f) CPV observables in $e^+e^- \to J/\psi \to \Xi^-\bar{\Xi}^+$. The dotted lines and the solid lines are the results for ST and DT experiments, respectively. For the asymmetries A_Ξ, $\Phi_{\rm CP}$, and A_Λ, also the analytic approximation is given: dashed-dotted lines and dashed lines are ST and DT results, respectively.

interesting since all production parameters are fixed and *CP*-test uncertainties depend only on α_b and α_B.

To understand the relative importance of the polarization and spin-correlation terms for the *CP* tests, one can compare the two above extreme cases. For example, the polarization in two ST experiments with N events that would lead to the same uncertainty of the $\Phi_{\rm CP}$ measurement as in the DT approach with N events is

$$|\mathbf{P}_B|^2 = \frac{\alpha_B^2(3-2\alpha_b^2)+3\alpha_b^2}{3+\alpha_B^2\alpha_b^2}.$$

For $\Xi \to \Lambda\pi$, this gives $|\mathbf{P}_B| = 0.80$.

Now, we will discuss the results specific for the $e^+e^- \to J/\psi \to \Xi\bar{\Xi}$ process. The relations for the ST experiment, realized as two independent measurements with N events each,[3] are still valid. The only difference is that now the results can be represented as a function of the electron-beam polarization P_e, and the average cascade polarization $|\mathbf{P}_\Xi|$ is calculated using Eq. (43). The results in the analytic approximation for the *A*-type observables corresponding to the ones in Fig. 7(a) are shown in Fig. 9(a). Since even for

[3]Of course, this is not the way one does the experiment since both the baryon and antibaryon decays can be measured simultaneously.

TABLE VI. Correlation matrix for the asymmetries and averages in the $e^+e^- \to J/\psi \to \Xi\bar{\Xi}$ process with $P_e = 0.8$ for DT. Input parameters are $\langle\alpha_\Xi\rangle = -0.373$, $\langle\phi_\Xi\rangle = 0.016$, and $\langle\alpha_\Lambda\rangle = 0.760$. The error is the last significant digit unless specified explicitly, and only the results statistically different from zero are shown.

	$\Delta\Phi$	$\langle\alpha_\Xi\rangle$	$\langle\phi_\Xi\rangle$	$\langle\alpha_\Lambda\rangle$	A_Ξ	A_Λ	$\Phi_{\rm CP}$	P_e
α_ψ	−0.128	⋯	0.011	−0.008	⋯	−0.017(2)	⋯	−0.031
$\Delta\Phi$		0.009	0.009	−0.071(2)	⋯	⋯	⋯	0.191(3)
$\langle\alpha_\Xi\rangle$			−0.021(4)	0.078(3)	⋯	⋯	⋯	0.037
$\langle\phi_\Xi\rangle$				−0.032	⋯	⋯	⋯	−0.005
$\langle\alpha_\Lambda\rangle$					⋯	⋯	⋯	−0.455

the $P_e = 0$ the average polarization of the cascades is not zero, all the three *CP* tests are possible. For the average values of the decay parameters, we do not provide approximate analytic results since the corresponding information matrix elements are correlated and in general multidimensional matrices have to be inverted to obtain uncertainties. Therefore, likely, such an analytic solution will not provide better understanding of the interrelations between the parameters. The numeric results for uncertainties of $\langle\alpha_\Xi\rangle$, $\langle\phi_\Xi\rangle$, and $\langle\alpha_\Lambda\rangle$ are shown in Figs. 10(a)–10(c) both for ST- and DT-type experiments. For the ST experiments, the uncertainty improves much more than for DT experiments. This difference is understood by the fact that the uncertainties in the DT experiment have a contribution from the spin-correlation term that depends weakly on P_e (see Fig. 5). The numerical results for the A_Ξ, $\Phi_{\rm CP}$, and A_Λ are given in Figs. 10(d)–10(f) and compared to the analytic approximations, which represent well the results specially for the Ξ decay CPV tests. As a cross-check of the calculations, we provide in Table VI the full correlation matrix of all parameters using the full numerical calculations for $P_e = 0.8$. Significant values of some of the correlation terms, like $\Delta\Phi$–α_ψ or $\langle\alpha_\Lambda\rangle$–$P_e$, indicate that it might be difficult to provide an intuitive picture of the relations between all the parameters. However, the numerical results confirm that the *CP*-violation variables are almost uncorrelated with the other variables and support our assumption that they can be analyzed separately.

Finally, it is interesting to consider a general two-step process $B \to b\pi$ in the low- and high-energy limits

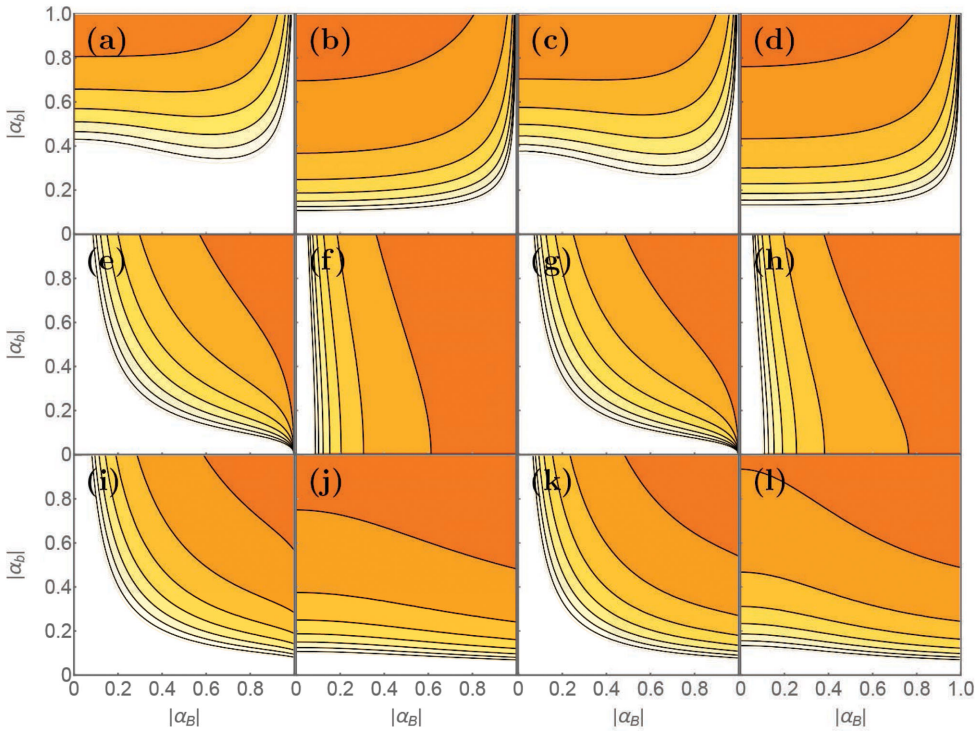

FIG. 11. Statistical uncertainties σ_C of (a)–(d) $\Phi_{\rm CP}$, (e)–(h) A_B, and (i)–(l) A_b measurements in the $e^+e^- \to \gamma^* \to B\bar{B}$ process with two-step B-baryon decays in the LE limit ($\alpha_\psi = 0$ and $\Delta\Phi = 0$) and (HE) limit ($\alpha_\psi = 1$) as the function of α_B and α_b treated as free parameters. The columns from left are (LE limit, $P_e = 0$), (LE limit, $P_e = 1$), (HE limit, $P_e = 0$), and (HE limit, $P_e = 1$). The same color scale as in Fig. 8 is used. The white regions in the plots correspond to uncertainties $\sigma_C(\ldots) > 15$.

(introduced in Sec. III) for a single photon $e^+e^- \to B\bar{B}$ annihilation process. These cases might be of interest for close to threshold charm baryon studies or baryon-antibaryon production experiments at high energies. In the LE limit ($\alpha_\psi = 0$, $\beta_\psi = 0$, $\gamma_\psi = 1$), the terms $\langle \mathbb{P}_B^2 \rangle$ and $\langle \mathbb{S}_{B\bar{B}}^2 \rangle$ are $2P_e^2$ and 1, respectively. In the HE limit ($\alpha_\psi = 1$, $\beta_\psi = 0$, $\gamma_\psi = 0$), they are equal to $6(1-\pi/4)P_e^2$ and $3(\pi/2-1)$, respectively. In both cases, the spin-correlation terms do not depend on the electron polarization, and the $\langle \mathbb{P}_B^2 \rangle$ terms are proportional to P_e^2. A comparison of the uncertainties for $P_e = 0$ and $P_e = 1$ in the DT-experiment setting is presented in Fig. 11. The conclusion is that the polarization helps to reach better precision in both cases, and the improvement is qualitatively similar.

VI. EXPERIMENTAL CONSIDERATIONS

The benefits of a large electron-beam polarization for *CP*-violation studies should be clear by now. Here, we discuss three additional aspects related to the detection technique, which should be considered when planning such an experiment:

(a) combination of the ST and DT datasets including detection efficiency and background aspects,
(b) polar angle dependence of uncertainty and the detection efficiency,
(c) Implications of the discussed collision scheme with large-crossing angle.

A. Combination of ST and DT measurements

In general, the best precision can be achieved by combining three nonoverlapping event sets. The first set includes the DT events where both the B and $\bar{B}$ decay chains are reconstructed. The remaining events can be divided into two ST sets where $B(\bar{B})$ decay is fully reconstructed but not the corresponding $\bar{B}(B)$. The efficiencies of the B, $\bar{B}$, and $B\bar{B}$ sets are denoted as ϵ_B, $\epsilon_{\bar{B}}$, and $\epsilon_{B\bar{B}}$, respectively. The efficiencies can depend on the vector $\boldsymbol{\xi}$ of the kinematic variables, but not on the global reaction parameters given by the $\boldsymbol{\omega}$ vector. Since we discuss improvements with respect to the DT-type experiment, ϵ_B is given by the ratio between the detection efficiencies of the DT and ST cases. We also neglect any efficiency dependence on the kinematic variables. We recollect that the information in the DT experiment, based on N reconstructed events, is given by Eq. (70):

$$\mathcal{I}_0^{\mathrm{DT}}(\omega_i, \omega_j) = N[\mathbb{a}_{ij} + \mathbb{b}_{ij}\langle \mathbb{P}_B^2 \rangle + \mathbb{c}_{ij}\langle \mathbb{S}_{B\bar{B}}^2 \rangle].$$

For the two-step process $\mathbb{a}_{ij}$, $\mathbb{b}_{ij}$, and $\mathbb{c}_{ij}$ can be read from Eqs. (71)–(74). For the single-step process, only A_B can be measured $\mathbb{a}_{A_B} = \mathbb{c}_{A_B} = 0$ and $\mathbb{b}_{A_B} = 1/3$:

$$\mathcal{I}_0(A_B) = N\frac{1}{3}\langle \mathbb{P}_B^2 \rangle.$$

The information provided by the two additional ST sets is

$$\mathcal{I}_0^{\mathrm{ST}}(\omega_i, \omega_j) = N\frac{1-\epsilon_B\mathcal{B}}{\epsilon_B\mathcal{B}}[2\mathbb{a}_{ij} + \mathbb{b}_{ij}\langle \mathbb{P}_B^2 \rangle], \quad (80)$$

where the branching fraction product of the decay sequence is $\mathcal{B}$ and equal detection efficiencies $\epsilon_B = \epsilon_{\bar{B}}$ are assumed. The interpretation of the above equation is that an additional $2N/(\epsilon_B\mathcal{B})$ events are added from the two ST sets. Therefore, the information of the combined ST and DT experiment (ST&DT) is the sum of the two independent measurements:

$$\mathcal{I}_0^{\mathrm{ST\&DT}}(\omega_i, \omega_j) = N\left[\frac{2-\epsilon_B\mathcal{B}}{\epsilon_B\mathcal{B}}\mathbb{a}_{ij} + \frac{1}{\epsilon_B\mathcal{B}}\mathbb{b}_{ij}\langle \mathbb{P}_B^2 \rangle + \mathbb{c}_{ij}\langle \mathbb{S}_{B\bar{B}}^2 \rangle\right]. \quad (81)$$

In the single-step decays, the $\sigma_C(A_{\mathrm{CP}})$ dependence on the electron-beam polarization for both ST and DT experiments is approximately given by Eq. (65). The A_Λ uncertainties for ST, DT, and the combined $e^+e^- \to J/\psi \to \Lambda\bar{\Lambda}$ measurement are plotted in Fig. 12 as the function of P_e. Two cases of the detection efficiencies $\epsilon_B = 1$ and $\epsilon_B = 0.5$ are considered, and $\mathcal{B}(\Lambda \to p\pi^-) = 0.64$ is used. For the case with the reconstruction efficiency of 0.5, a two-times improvement of σ_C is achieved for the combination, compared to the DT measurement only. Of course, a detailed feasibility study which includes the detector response will be needed to determine the efficiency which can be obtained for the combined DT and ST measurement.

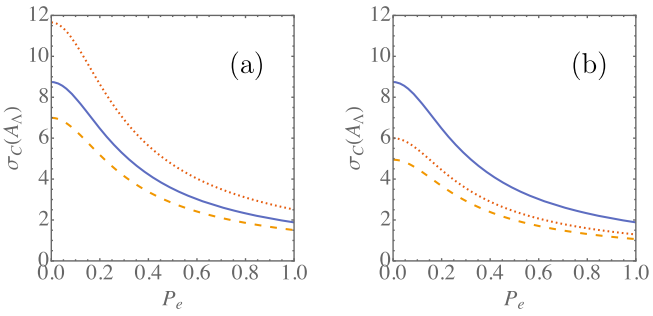

FIG. 12. Statistical uncertainties $\sigma_C(A_\Lambda)$ for the $e^+e^- \to J/\psi \to \Lambda\bar{\Lambda}$ process as a function of the electron-beam polarization P_e. The solid-blue lines represent DT measurement. The dotted-red lines represent contribution from ST events which do not contribute to the DT event class (statistically independent ST events). The orange-dashed lines represent the result from the combination of the two event classes. The decay branching fraction is $\mathcal{B} = 0.64$ [28]. The detection efficiency of the Λ decay was assumed to be (a) $\epsilon_\Lambda = \bar{\epsilon}_\Lambda = 1$ and (b) $\epsilon_\Lambda = \bar{\epsilon}_\Lambda = 0.5$. The results are normalized to the number of the DT events.

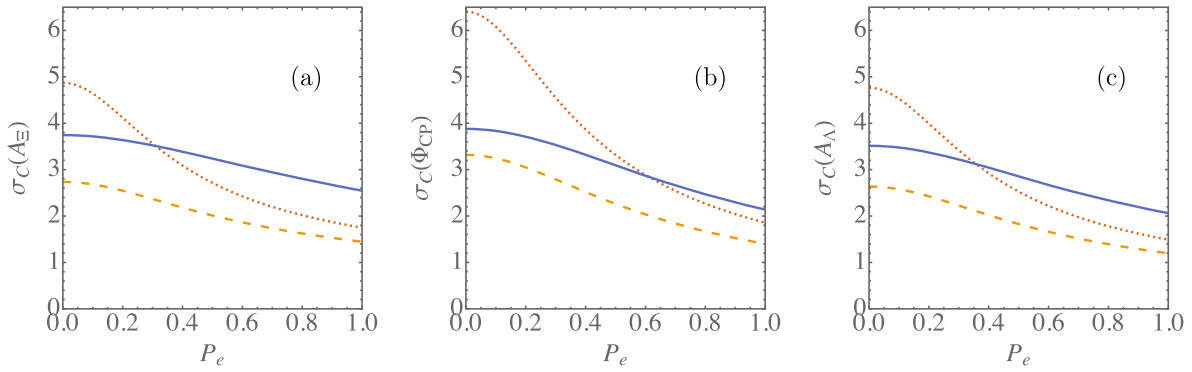

FIG. 13. Statistical uncertainties, σ_C, for the CP-violation observables in the $\Xi^- \to \pi^-\Lambda(\to p\pi^-) + \text{c.c.}$ decay sequences from the $e^+e^- \to J/\psi \to \Xi\bar{\Xi}$ process: (a) $\sigma_C(A_\Xi)$, (b) $\sigma_C(\Phi_{CP})$, and (c) $\sigma_C(A_\Lambda)$ as a function of electron beam polarization P_e. The solid-blue lines represent DT measurement. The dotted-red lines represent contribution from ST events which do not contribute to the DT event class (statistically independent ST events). The orange-dashed lines represent the result from the combination of the two event classes. The detection efficiency of the Ξ-decay sequence was assumed $\epsilon_\Xi = \bar{\epsilon}_\Xi = 0.5$ and branching fraction of the complete decay chain $\mathcal{B} = 0.64$. The results are normalized to the number of the DT events.

An important background contribution which should be considered for the ST analysis of the $J/\psi \to \Lambda\bar{\Lambda}$ events is $J/\psi \to pK^-\bar{\Lambda} + \text{c.c.}$ with $\mathcal{B} = (8.6 \pm 1.1) \times 10^{-4}$ [28] as it will have a similar final-state topology as the signal channel. Similar experimental considerations will also hold for the $J/\psi \to \Sigma\bar{\Sigma}$ two-body decay channels.

The results for A_Ξ and Φ_{CP} in the $e^+e^- \to J/\psi \to \Xi\bar{\Xi}$ are shown in Fig. 13. For the two-step decays, the increasing beam polarization improves the ST uncertainties much faster compared to the corresponding DT uncertainties. For the polarization of $P_e = 0.8$, the uncertainty of the ST experiment is better if we assume realistic efficiency of 50% deduced from a comparison of the BESIII ST [86] and DT [32] analyses.

Furthermore, the nonreducible backgrounds for the ST event samples are also expected to be low. The background channels to be considered are $J/\psi \to \gamma\eta_c(\to\Xi^-\bar{\Xi}^+)$, $J/\psi \to \Xi(1530)^-\bar{\Xi}^+ \to \Xi^-\pi^0\bar{\Xi}^+$, and $J/\psi \to \Lambda\pi^-\bar{\Lambda}\pi^+$. While the first two channels can be suppressed using event kinematics variables, the third can be reduced by requiring a nonzero decay length for the $\Xi \to \Lambda\pi$ decay candidates. For the DT method, the background contribution is 0.25%, and for ST, the background is at the percent level, while roughly three times more ST events can be reconstructed compared to DT.

B. Polar-angle efficiency dependence

Detectors at electron-positron colliders experiments have approximate cylindrical symmetry with axis along the beam directions (considerations for large-crossing angle are discussed in a separate paragraph) and uniform detection efficiency in the azimuthal angle. However, the polar-angle coverage is limited. For example, in the BESIII experiment, $|\cos\theta| < 0.93$ for tracks of charged particles. The hyperons decay some centimeters away from the interaction point, and the final-state particles with large $|\cos\theta|$ values have low transverse momenta, which are more difficult to reconstruct. These effects reduce the reconstruction efficiency at large values of $|\cos\theta|$.

The event yield is a product of the efficiency and the differential cross section of the $e^+e^- \to B\bar{B}$ process $d\Gamma/d\Omega \propto (1 + \alpha_\psi \cos^2\theta)$ as shown in Eq. (39). Since both $J/\psi \to \Lambda\bar{\Lambda}$ and $J/\psi \to \Xi^-\bar{\Xi}^+$ have $\alpha_\psi > 0$ (Table V), the (anti)hyperons and the decay (anti)nucleons are more likely emitted in the forward and backward directions. The uncertainty as a function of the production angle $\cos\theta$ can be obtained by replacing the production tensor $\langle C^2\rangle_{\mu\nu}$ by the normalized spin correlation matrix $C^2_{\mu\nu}/C^2_{00}$. The numerical expressions for the functions $\mathbb{P}^2_B(\cos\theta)$ and $\mathbb{S}^2_{B\bar{B}}(\cos\theta)$ are given in Appendix D. The results are shown in Fig. 14 for $\sigma_C(A_\Lambda)$ in DT experiments in $e^+e^- \to J/\psi \to \Lambda\bar{\Lambda}$ and $e^+e^- \to J/\psi \to \Xi\bar{\Xi}$ for different values of the electron beam polarization. Corresponding plots for $\sigma_C(\Phi_{CP})$ in the $e^+e^- \to J/\psi \to \Xi\bar{\Xi}$ DT and combined DT&ST measurements are shown in Fig. 15.

C. Large-angle collision scheme

The SCTF will use crab-waist collision scheme, meaning larger crossing angle than at BEPCII (22 mrad). The presently considered crossing angle is 60 mrad [34,35]. However, in Ref. [40], much larger crossing angles, up to 500 mrad, are considered in conjunction with a novel c.m. energy monochromatization scheme. The monochromatization could increase the number of the J/ψ events, and therefore it is worthwhile to discuss some of the consequences of such collision arrangement for the acceptance in the hyperon CP-violation tests.

In such collision scheme, the detector reference frame is significantly different from the electron-positron c.m.

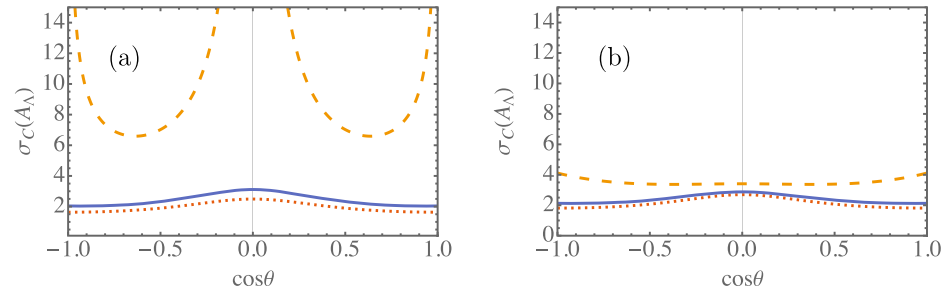

FIG. 14. Uncertainties $\sigma_C(A_\Lambda)$ in the DT measurement in (a) $e^+e^- \to J/\psi \to \Lambda\bar{\Lambda}$ and (b) $e^+e^- \to J/\psi \to \Xi\bar{\Xi}$ processes as a function of the production angle $\cos\theta$ where the dashed line shows $P_e = 0$, the solid line is for $P_e = 0.8$, and the dotted line represents $P_e = 1$.

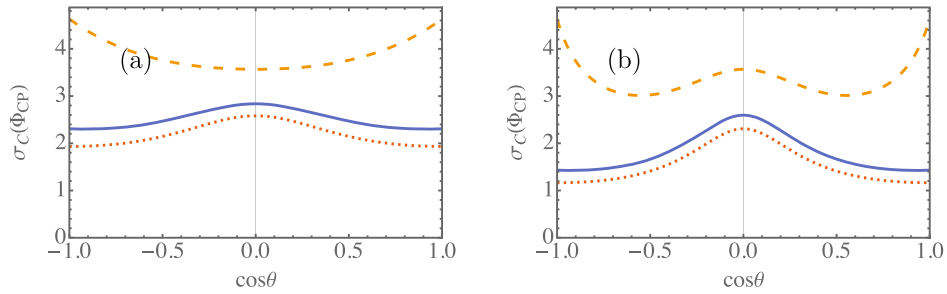

FIG. 15. Uncertainties $\sigma_C(\Phi_{CP})$ as a function of the production angle $\cos\theta$ for (a) DT and (b) DT&ST with 50% efficiency experiment where the dashed line (orange) shows $P_e = 0$, the solid line (blue) is for $P_e = 0.8$, and the dotted line (red) represents $P_e = 1$.

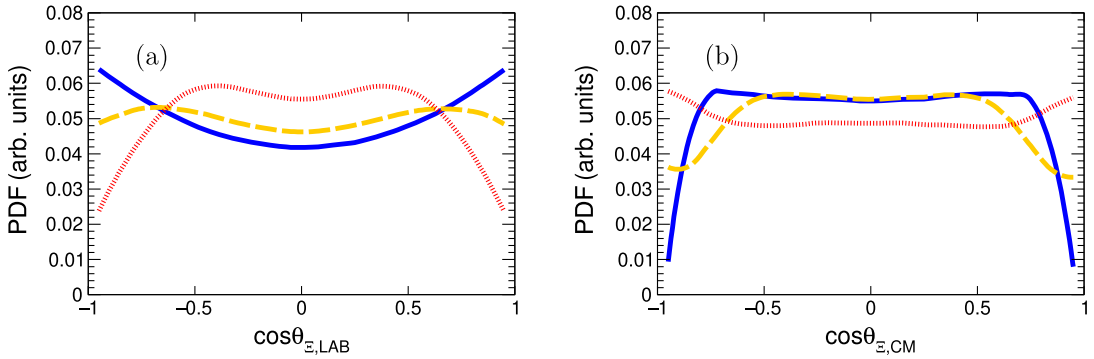

FIG. 16. Production angle distribution for beam-crossing angles 0 rad (blue solid), 0.3 rad (orange dashed), and 0.5 rad (red dotted). (a) The Ξ production angle in the detector frame. (b) The Ξ production angle in the electron-positron c.m. frame for the events where all six charged tracks are accepted in the detector $|\cos\theta_{\rm LAB}| < 0.93$.

system. This has impact on both angular acceptance and the detection efficiency as a function of the measured-particles momenta, and it has to be considered in the detector design. For example, the polar-angle, $\theta_{\rm LAB}$, distribution of Ξ^- in the detector rest frame is given in Fig. 16(a) for the 0.0, 0.3, and 0.5 rad crossing angles. If the decay particles are measured only in the $|\cos\theta_{\rm LAB}| < 0.93$ range as in the BESIII detector, the observed Ξ production-angle distribution in the electron-positron c.m. system is as in Fig. 16(b). A large beam-crossing angle will also significantly affect the azimuthal-angle distribution in the detector reference system, as shown in Fig. 17(a). This will introduce acceptance effects depending on the azimuthal angle that should be corrected for in the analysis. However, the acceptance effects should be easy to disentangled from the process angular distributions since in the electron-positron collision rest frame the azimuthal distribution has to be flat. In addition, an improved particle identification algorithm will be needed since the momentum distributions of the final-state protons and pions will overlap with each other, as shown in Fig. 17(b), while for the electron-positron rest frame collision scheme, a momentum range separation was sufficient.

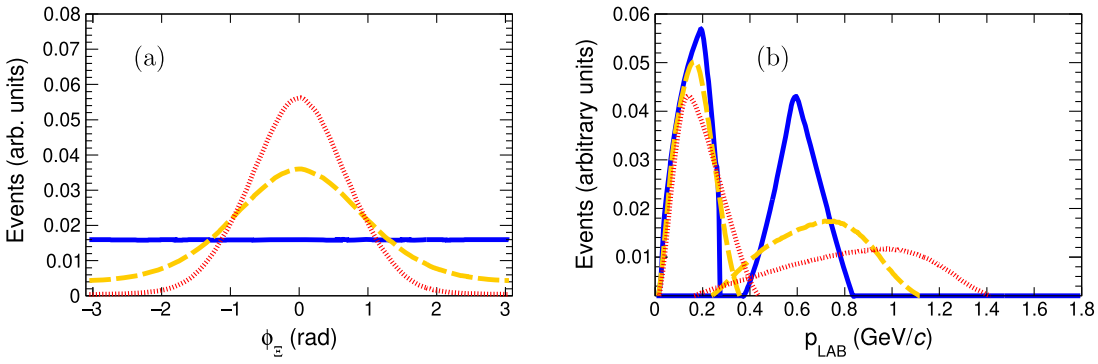

FIG. 17. (a) Azimuthal distribution of $\Xi_{\rm LAB}$ and (b) momentum distributions for all final-state particles for beam scattering angles 0 rad (blue solid), 0.3 rad (orange dashed), and 0.5 rad (red dotted).

VII. OUTLOOK

We have advocated the importance of CPV studies in hyperon decays as a complementary tool to the studies in kaon processes. Using recent experimental results, we have revised and updated the amplitudes of the Λ and Ξ hadronic two-body decays.

The main part of this report discusses the implications of the polarized-electron beams for CPV tests in the nonleptonic hyperon decays at SCTF, using entangled baryon-antibaryon pairs from J/ψ decays with datasets of 10^{12} J/ψ events. The use of the polarization, together with additional improvements of the analysis techniques, shows the potential to reach a precision compatible with the size of the predicted SM signal.

Using an analytical approximation for the Fisher information matrices of the CPV observables, we can understand how the precision of such measurements depends on the polarization and spin-correlation terms in the production processes. Some of the obtained analytical results can be directly extended to charm baryon CPV studies. At SCTF, they can be studied in close-to-threshold $e^+e^- \to B\bar{B}$ processes. For such processes, the analytic results of Secs. IV and V can be taken as a starting point. The main difference in the strategy for charmed baryons is due to the fact that the branching fractions for two-body nonleptonic decays are small, and the DT analysis likely will not be feasible.

In addition to the $e^+e^- \to B\bar{B}$ processes, the HyperCP-type experiments can be an interesting option for CP tests and decay parameter determination, provided that sources of (anti)baryons with large initial polarization are available. Possible candidate processes are semileptonic decays of charmed baryons $\Xi_c^0 \to \Xi^-\ell^+\nu_\ell$ or two-body hadronic decays like $\Xi_c^0 \to \Xi^-\pi^+$ with large value of the decay parameter $\alpha = 0.63(3)$ [87] and relatively large branching fraction 1.2% [28]. For such studies, unpolarized charmed baryons that are abundantly produced at the LHC in pp collisions can be used. Again, our analytic formulas can be used to provide a first estimate of the statistical uncertainties for such experiments.

We have left out a potentially interesting discussion of the uncertainties of the decay parameters α_D and ϕ_D. For example the α_D parameter is correlated at least with the production parameters α_ψ, $\Delta\Phi$ and P_e and the determination of the uncertainty requires inverting non-diagonal 4×4 information matrix. Therefore the results of the analytic approximation will be not much easier to interpret than the full numerical calculations. The same is valid for the production parameters α_ψ and $\Delta\Phi$ that are relevant for the experiments where the goal is to study the properties of the production process. Usually, such experiments have a limited number of the collected events, and analysis is done assuming the decay parameters are known.

ACKNOWLEDGMENTS

This work was supported in part by National Natural Science Foundation of China (NSFC) under Contract No. 11935018 and Polish National Science Centre through Grant No. 2019/35/O/ST2/02907. P. A. is grateful for the support from Olle Engkvist Foundation and Lundström-Åman Foundation. V. B. contribution is supported by the CAS President's International Fellowship Initiative (PIFI) (Grant No. 2021PM0014). In addition, a support from the Swedish Research Council under Grant No. 2021-04567 and the European Union's Horizon 2020 research and innovation programme under the grant STRONG-2020 Grant No. 824093 is acknowledged.

APPENDIX A: ISOSPIN DECOMPOSITION

Here, we evaluate the $\Delta I = 1/2$ and $\Delta I = 3/2$ components of the $\Lambda \to N\pi$ and $\Xi \to \Lambda\pi$ amplitudes. As in the main text, we *assume* isospin symmetry for the elementary weak decay process but take into account the impact of isospin-violating mass splittings in the kinematics. The basic parameters in the Feynman matrix element $\bar{u}_b(g_S - \gamma_5 g_P)u_B$ of the weak decay of a spin-1/2 baryon B into another spin-1/2 baryon b and a pion are related to the partial-wave amplitudes S and P via

$$g_S = S, \qquad g_P = P\frac{E+M}{|\mathbf{q}|}, \tag{A1}$$

where $|\mathbf{q}|$, E, and M stand for the momentum, energy, and mass, respectively, of b in the rest frame of B. Further consideration on $g_{S,P}$ is provided in Appendix B (see also minireview 79.2., "Hyperon nonleptonic decays," in Ref. [28]). The isospin breaking mentioned above arises from the p-wave kinematical factor $|\mathbf{q}|/(E+M)$ as well as the phase-space volume.

Suppose we have two decay modes, labeled I and II, connected by isospin symmetry (e.g., $\Lambda \to p\pi^-$ and $\Lambda \to n\pi^0$). Our isospin-symmetry assumption for the basic parameters is then expressible as

$$(g_S)_{\rm I} = (g_S)_{\rm II}, \qquad (g_P)_{\rm I} = (g_P)_{\rm II}. \tag{A2}$$

In view of Eqs. (A1) and (A2), the S and P amplitudes $S_{\rm I,II}$ and $P_{\rm I,II}$, respectively, for the two processes, including corrections $\Delta_{\rm I}$ and $\Delta_{\rm II}$ due to different masses in the kinematical factors, can be written as

$$S_{\rm I} = S_{\rm II}, \quad P_{\rm I}(1+\Delta_{\rm I}) =: P_{\rm I}\frac{E_{\rm I}+M_{\rm I}}{|\mathbf{q}_{\rm I}|}\frac{|\bar{\mathbf{q}}|}{\bar{E}+\bar{M}} = P_{\rm II}(1+\Delta_{\rm II}), \tag{A3}$$

where $|\bar{\mathbf{q}}|/(\bar{E}+\bar{M})$ contains only isospin-averaged masses,[4] which ensures that $|\Delta_{\rm I,II}| \ll 1$. For $\Lambda \to p\pi^-$ ($[\Lambda p]$), $\Lambda \to n\pi^0$ ($[\Lambda n]$), $\Xi^- \to \Lambda\pi^-$ ($[\Xi-]$), and $\Xi^0 \to \Lambda\pi^0$ ($[\Xi 0]$), the Δs are calculated to be at most a couple of percent in size, specifically

$$\Delta_{[\Lambda p]} = 0.007769(3), \qquad \Delta_{[\Lambda n]} = -0.023631(6), \tag{A4}$$

$$\Delta_{[\Xi-]} = -0.0201(9), \qquad \Delta_{[\Xi 0]} = 0.011(1). \tag{A5}$$

The isospin decomposition, in notation similar to Ref. [88], of the $L = S$, P amplitudes for $\Lambda \to N\pi$ into their $\Delta I = 1/2, 3/2$ components reads

$$\begin{aligned} L_{[\Lambda p]} &= -\sqrt{\frac{2}{3}}L_{1,1}\exp(i\xi^L_{1,1} + i\delta^L_1) \\ &\quad + \sqrt{\frac{1}{3}}L_{3,3}\exp(i\xi^L_{3,3} + i\delta^L_3), \\ L_{[\Lambda n]} &= \sqrt{\frac{1}{3}}L_{1,1}\exp(i\xi^L_{1,1} + i\delta^L_1) \\ &\quad + \sqrt{\frac{2}{3}}L_{3,3}\exp(i\xi^L_{3,3} + i\delta^L_3), \end{aligned} \tag{A6}$$

where in the $L = P$ case $P_{[\Lambda p]}$ and $P_{[\Lambda n]}$ on the left-hand sides are to be replaced by $(1+\Delta_{[\Lambda p]})P_{[\Lambda p]}$ and $(1+\Delta_{[\Lambda n]})P_{[\Lambda n]}$, respectively, as per the discussion in the previous paragraph. Analogously, for the $\Xi \to \Lambda\pi$ channels, one has

$$\begin{aligned} L_{[\Xi-]} &= L_{1,2}\exp(i\xi^L_{1,2} + i\delta^L_2) + \frac{1}{2}L_{3,2}\exp(i\xi^L_{3,2} + i\delta^L_2), \\ L_{[\Xi 0]} &= \frac{1}{\sqrt{2}}L_{1,2}\exp(i\xi^L_{1,2} + i\delta^L_2) - \frac{1}{\sqrt{2}}L_{3,2}\exp(i\xi^L_{3,2} + i\delta^L_2), \end{aligned} \tag{A7}$$

with $P_{[\Xi-]} \to (1+\Delta_{[\Xi-]})P_{[\Xi-]}$ and $P_{[\Xi 0]} \to (1+\Delta_{[\Xi 0]})P_{[\Xi 0]}$. Incorporating Eqs. (A6) and (A7) into Eqs. (3) and (5); employing the experimental values of the pertinent α parameters, partial rates, phase shifts, and masses; and dropping the tiny weak phases ξ^L_J, we can then extract $L_{2\Delta I,2I}$ for the Λ and Ξ modes.

In the Ξ case, due to the fact that only one phase-shift difference, $\delta^P_2 - \delta^S_2$, is involved, it turns out to be possible to derive $L_{1,2}$ and $L_{3,2}$ analytically in terms of empirically known quantities, but we will not include the lengthy expressions in this paper. To evaluate them numerically, we adopt the boldfaced $\alpha_{[\Xi-]}$ and $\alpha_{[\Xi 0]}$ numbers quoted in Table II as well as the appropriate masses and partial rates from Ref. [28]. As for the strong phases, after combining the relation $\tan(\delta^P_2 - \delta^S_2) = \sin\phi\sqrt{1-\alpha^2}/\alpha$ with the measured α and ϕ parameters for the Ξ decays listed in Table II, we find the average experimental value $\delta^P_2 - \delta^S_2 = 1(4)°$, which is consistent with zero and perhaps suggestive of it being considerably smaller than the pion-nucleon phase shifts relevant to the Λ and Σ decays (given in Table III).[5] Putting things together, we collect the resulting $L_{1,2}$, $L_{3,2}$, and $L_{3,2}/L_{1,2}$ in Table VII, all the Ls written in units of the Fermi constant $G_{\rm F}$ times the charged pion's squared mass. Evidently, the size of $S_{3,2}$ relative to $S_{1,2}$ is 5%, while $P_{3,2}$ is consistent with zero (less than 3% of $P_{1,2}$ within one standard deviation).

Compared to their Ξ counterparts, the Λ decay amplitudes are more complicated, having four different strong phases, and consequently it does not seem feasible to arrive at analytical formulas for $L_{1,1}$ and $L_{3,3}$. Nevertheless, one can still determine them by means of numerical computation. Thus, with the boldfaced $\alpha_{[\Lambda p]}$ and $\alpha_{[\Lambda n]}$ entries in Table II, the $\Lambda \to N\pi$ phases in Table III, and masses and partial rates from Ref. [28], we obtain the numbers displayed in the bottom row of Table VII. It shows that the $\Delta I = 3/2$ components of S and P are 3% and 5% of the corresponding $\Delta I = 1/2$ ones in size.

[4]Explicitly, these are $\bar{M}_N = (M_p + M_n)/2$, $\bar{M}_\Xi = (M_{\Xi^-} + M_{\Xi^0})/2$, and $\bar{M}_\pi = (2M_{\pi^+} + M_{\pi^0})/3$ for the isospin nonsinglets.

[5]By contrast, as remarked in Sec. II B, recent theoretical studies have predicted that $\delta^P_2 - \delta^S_2$ might be significantly bigger [63,65], as much as 9°.

TABLE VII. Amplitudes, in dimensionless units of $G_F m_{\pi^+}^2$, for the $\Delta I = 1/2$ and $\Delta I = 3/2$ transitions, and the corresponding $(\Delta I = 3/2)/(\Delta I = 1/2)$ amplitude ratios, in the Λ- and Ξ-hyperon nonleptonic decays.

	$\Delta I = 1/2$		$\Delta I = 3/2$		$(\Delta I = 3/2)/(\Delta I = 1/2)$	
Decay mode	S	P	S	P	S ratio	P ratio
$\Xi \to \Lambda\pi$	−2.05(1)	0.386(5)	0.11(2)	−0.002(8)	−0.05(1)	−0.005(21)
$\Lambda \to N\pi$	−1.718(8)	−0.759(2)	−0.050(9)	0.036(9)	0.029(6)	−0.05(1)

If one is interested merely in the relative size of the different amplitudes, it is possible to infer their ratios approximately from the αs and squared amplitudes upon expanding them to linear order in the $\Delta I = 3/2$ components or the Δ_D parameters, which have effects of comparable size on the $\Delta I = 1/2$ contributions. This complementary procedure also helps cross-check Table VII.

In this approximation, for the Ξ modes, we have the α combinations

$$\alpha_{[\Xi]} := \frac{2\alpha_{[\Xi-]} + \alpha_{[\Xi 0]}}{3} = 2\hat{S}_1\hat{P}_1\cos(\delta_2^P - \delta_2^S)\left[1 + \frac{1}{3}(1 - 2\hat{S}_1^2)(2\Delta_{[\Xi-]} + \Delta_{[\Xi 0]})\right] \stackrel{\text{exp}}{=} -0.368(4), \tag{A8}$$

$$\frac{\alpha_{[\Xi-]} - \alpha_{[\Xi 0]}}{\alpha_{[\Xi]}} = (1 - 2\hat{S}_1^2)\left(\frac{3}{2}\frac{\hat{S}_3}{\hat{S}_1} - \frac{3}{2}\frac{\hat{P}_3}{\hat{P}_1} + \Delta_{[\Xi-]} - \Delta_{[\Xi 0]}\right) \stackrel{\text{exp}}{=} 0.092(25), \tag{A9}$$

where $\hat{L}_k = L_{k,2}/(S_{1,2}^2 + P_{1,2}^2)^{1/2}$ for $L = S,\ P$ and $k = 1,\ 3$, implying that $\hat{S}_1^2 + \hat{P}_1^2 = 1$. We also have the squared amplitudes

$$\begin{aligned} |\mathcal{A}_{[\Xi-]}|^2 &= S_{1,2}^2 + (1 - 2\Delta_{[\Xi-]})P_{1,2}^2 + S_{1,2}S_{3,2} + P_{1,2}P_{3,2}, \\ |\mathcal{A}_{[\Xi 0]}|^2 &= \frac{1}{2}S_{1,2}^2 + \frac{1}{2}(1 - 2\Delta_{[\Xi 0]})P_{1,2}^2 - S_{1,2}S_{3,2} - P_{1,2}P_{3,2}, \end{aligned} \tag{A10}$$

where the left-hand sides are connected via Eq. (5) to the observed rates $\Gamma(\Xi^- \to \Lambda\pi^-)$ and $\Gamma(\Xi^0 \to \Lambda\pi^0)$, respectively, leading to

$$\frac{1}{2}\frac{\Gamma(\Xi^- \to \Lambda\pi^-) - 2\Gamma(\Xi^0 \to \Lambda\pi^0)r_\Xi}{\Gamma(\Xi^- \to \Lambda\pi^-) + \Gamma(\Xi^0 \to \Lambda\pi^0)r_\Xi} = \hat{S}_1\hat{S}_3 + \hat{P}_1\hat{P}_3 - \frac{2}{3}(\Delta_{[\Xi-]} - \Delta_{[\Xi 0]})\hat{P}_1^2 \stackrel{\text{exp}}{=} -0.050(11), \tag{A11}$$

where $r_\Xi = 1.0270(18)$ is the ratio of phase space volumes of the two modes. From Eq. (A8), we extract $\hat{S}_1 = -0.9827(4)$, and hence $\hat{P}_1 = (1 - \hat{S}_1^2)^{1/2} = 0.185(2)$, with which we solve Eqs. (A9) and (A11) for $\hat{S}_3 = 0.05(1)$ and $\hat{P}_3 = -0.001(4)$, and so we get $\hat{S}_3/\hat{S}_1 = -0.05(1)$ and $\hat{P}_3/\hat{P}_1 = -0.007(20)$. These results can be seen to be compatible with the $\Xi \to \Lambda\pi$ entries in Table VII.

Similarly, in the Λ case, we have

$$\alpha_{[\Lambda]} := \frac{2\alpha_{[\Lambda p]} + \alpha_{[\Lambda n]}}{3} = 2\tilde{S}_1\tilde{P}_1\cos(\delta_1^P - \delta_1^S)\left[1 + \frac{1}{3}(1 - 2\tilde{S}_1^2)(2\Delta_{[\Lambda p]} + \Delta_{[\Lambda n]})\right] \stackrel{\text{exp}}{=} 0.734(6), \tag{A12}$$

$$\frac{\alpha_{[\Lambda p]}-\alpha_{[\Lambda n]}}{\alpha_{[\Lambda]}}=\frac{-3}{\sqrt{2}}\left[\frac{\tilde{S}_3}{\tilde{S}_1}\frac{\cos(\delta_1^P-\delta_3^S)}{\cos(\delta_1^P-\delta_1^S)}+\frac{\tilde{P}_3}{\tilde{P}_1}\frac{\cos(\delta_1^S-\delta_3^P)}{\cos(\delta_1^P-\delta_1^S)}\right]+3\sqrt{2}[\tilde{S}_1\tilde{S}_3\cos(\delta_1^S-\delta_3^S)+\tilde{P}_1\tilde{P}_3\cos(\delta_1^P-\delta_3^P)]$$
$$+(1-2\tilde{S}_1^2)(\Delta_{[\Lambda p]}-\Delta_{[\Lambda n]})$$
$$\stackrel{\text{exp}}{=}0.086(24), \tag{A13}$$

$$\frac{\Gamma(\Lambda\to p\pi^-)-2\Gamma(\Lambda\to n\pi^0)r_\Lambda}{\Gamma(\Lambda\to p\pi^-)+\Gamma(\Lambda\to n\pi^0)r_\Lambda}=-\sqrt{8}[\tilde{S}_1\tilde{S}_3\cos(\delta_1^S-\delta_3^S)+\tilde{P}_1\tilde{P}_3\cos(\delta_1^P-\delta_3^P)]-\frac{4}{3}(\Delta_{[\Lambda p]}-\Delta_{[\Lambda n]})\tilde{P}_1^2$$
$$\stackrel{\text{exp}}{=}-0.053(13), \tag{A14}$$

where $\tilde{L}_k=L_{k,k}/(S_{1,1}^2+P_{1,1}^2)^{1/2}$ for $L=S$, P and $k=1$, 3 and $r_\Lambda=0.965815(8)$ is the ratio of $\Lambda\to N\pi$ phase-space volumes. From Eq. (A12), we obtain $\tilde{S}_1=-0.915(2)$, and hence $\tilde{P}_1=-(1-\tilde{S}_1^2)^{1/2}=-0.404(4)$, with which we find $\tilde{S}_3=-0.027(5)$ and $\tilde{P}_3=0.019(6)$ from Eqs. (A13) and (A14) and consequently $\tilde{S}_3/\tilde{S}_1=0.029(6)$ and $\tilde{P}_3/\tilde{P}_1=-0.05(1)$. As expected, these are in line with the $\Lambda\to N\pi$ numbers in Table VII.

Finally, we illustrate how the knowledge about the $\Delta I=1/2,3/2$ components could improve the accuracy of estimating the β and ϕ parameters, which are linked to α by Eq. (8) and not all of which have been measured. Focusing on the Λ channels, for the βs, we can write, to first order in the $\Delta I=3/2$ amplitudes,

$$\frac{\beta_{[\Lambda p]}}{\alpha_{[\Lambda p]}}=\tan(\delta_1^P-\delta_1^S)+\frac{\tilde{P}_3\sin(\delta_1^P-\delta_3^P)}{\sqrt{2}\tilde{P}_1\cos^2(\delta_1^P-\delta_1^S)}-\frac{\tilde{S}_3\sin(\delta_1^S-\delta_3^S)}{\sqrt{2}\tilde{S}_1\cos^2(\delta_1^P-\delta_1^S)},$$
$$\frac{\beta_{[\Lambda n]}}{\alpha_{[\Lambda n]}}=\tan(\delta_1^P-\delta_1^S)-\frac{\sqrt{2}\tilde{P}_3\sin(\delta_1^P-\delta_3^P)}{\tilde{P}_1\cos^2(\delta_1^P-\delta_1^S)}+\frac{\sqrt{2}\tilde{S}_3\sin(\delta_1^S-\delta_3^S)}{\tilde{S}_1\cos^2(\delta_1^P-\delta_1^S)}, \tag{A15}$$

as the contributions linear in the Δ_D's cancel in the ratios. Upon applying these formulas and Eq. (8), with the boldfaced $\alpha_{[\Lambda p]}$ and $\alpha_{[\Lambda n]}$ values in Table II, the $\Lambda\to N\pi$ strong phases in Table III, and the above calculation of $\tilde{S}_{1,3}$ and $\tilde{P}_{1,3}$, we arrive at

$$\beta_{[\Lambda p]}=-0.100(2),\qquad \phi_{[\Lambda p]}=-0.153(3), \tag{A16}$$

$$\beta_{[\Lambda n]}=-0.083(3),\qquad \phi_{[\Lambda n]}=-0.115(7). \tag{A17}$$

If the $\Delta I=3/2$ terms in Eq. (A15) were neglected, we would instead get $\beta_{[\Lambda p]}=-0.097(2)$, $\phi_{[\Lambda p]}=-0.148(3)$, $\beta_{[\Lambda n]}=-0.089(3)$, and $\phi_{[\Lambda n]}=-0.123(6)$, which differ from their counterparts in Eqs. (A16) and (A17) by 3% and 7%, respectively. It is interesting to notice that the $\phi_{[\Lambda p]}$ prediction in Eq. (A16) is 20 times more precise than the direct measurement of $-0.113(61)$ quoted in Table II.

APPENDIX B: EFFECTIVE LAGRANGIAN AND PARAMETRIZATION OF AMPLITUDES

A Hermitian effective Lagrangian for the initial decay $B\to b\pi$ where all baryons have spin 1/2 is given by

$$\mathcal{L}=g_S i\bar{b}B\pi-g_S^* i\bar{B}b\bar{\pi}-g_P\bar{b}i\gamma_5 B\pi-g_P^*\bar{B}i\gamma_5 b\bar{\pi}. \tag{B1}$$

The g_S terms lead to s waves for the decay products, the g_P terms lead to p waves, and the g_S terms break parity symmetry, while the g_P terms do not. If g_S is real, then the g_S terms break P and C, but conserve CP symmetry. If g_P is real, then the g_P terms conserve C symmetry and therefore also CP. One can make g_P real and positive by moving its phase into a redefinition of the B-baryon field (and a redefinition of the discrete transformations by an additional phase). The CP symmetry is then conserved, if the parameter g_S is real.

Except for an irrelevant overall phase, one might write the decay matrix elements as

$$\mathcal{M}_{B\to b\pi}\sim\bar{u}_b(g_S-g_P\gamma_5)u_B,$$
$$\mathcal{M}_{\bar{B}\to\bar{b}\,\bar{\pi}}\sim\bar{v}_B(-g_S^*-g_P^*\gamma_5)v_b. \tag{B2}$$

This fits to the conventions of the Particle Data Group. Then, one reads off $S_{\text{ini}}\sim g_S$, $\bar{S}_{\text{ini}}\sim -g_S^*$, $P_{\text{ini}}\sim g_P$, and $\bar{P}_{\text{ini}}\sim g_P^*$, where the p waves pick up an additional phase-space factor that we have not displayed explicitly. The relations between partial-wave amplitudes and parameters from the Lagrangian suggest writing for the initial amplitudes

$$S_{\rm ini} = |S|e^{i\xi_S}, \qquad P_{\rm ini} = |P|e^{i\xi_P},$$
$$\bar{S}_{\rm ini} = -|S|e^{-i\xi_S}, \qquad \bar{P}_{\rm ini} = |P|e^{-i\xi_P}. \tag{B3}$$

Strictly speaking, ξ_P is not needed. What matters is the relative phase between S and P, which can be expressed via $\xi_S - \xi_P$ but equally well via ξ_S if one puts $\xi_P = 0$. In principle, phases can vary between 0 and 2π or $-\pi$ and π. However, an overall minus sign for all amplitudes would not lead to an observable consequence. Therefore, it is sufficient to consider $\xi_S - \xi_P \in [0, \pi)$ or $\in [-\pi/2, +\pi/2)$. If (B3) were the complete amplitudes, then one would always find $\bar{\alpha} = -\alpha$ and $\bar{\beta} = \beta$, irrespective of CP violation or conservation. For the case of CP symmetry, one would find $\beta = 0$.

This whole analysis leaves out final-state interactions. Rescattering is a nonlocal phenomenon that cannot be treated by a tree-level calculation using a local, Hermitian Lagrangian. Instead, one can use explicit loop calculations if one has a microscopic picture of the reaction, or one can use an Omnès-function matrix that parametrizes the final-state interactions. This is discussed in more detail in Appendix C.

APPENDIX C: TREATMENT OF FINAL-STATE INTERACTIONS

In the following, we discuss in some detail the treatment of final-state interactions for the main decays of the Λ and $\bar{\Lambda}$ baryons. The case of $\Xi^{0,-}$ decays is just simpler. Concerning the general treatment of final-state interactions, see also Refs. [89–93]. The hyperon decays that we study in the present work do not allow for many intermediate inelastic channels since the decaying strange quark is not very heavy. Decays of charm or bottom baryons would provide much more phase space and correspondingly contain many more open channels. Kinematically closed channels might become important if they are strong (e.g., resonance enhanced) and if their threshold is close to the studied invariant mass (e.g., this happens for the $f_0(980)$ and the kaon-antikaon threshold [94]). There are no non-strange resonances close to the Λ mass and no single-strange resonances close to the Ξ mass.

The relevant decay channels of Λ are $(p\pi^-)_S$, $(p\pi^-)_P$, $(n\pi^0)_S$, and $(n\pi^0)_P$, where the subscript denotes the partial wave. It is more convenient to build linear combinations with respect to the isospin of the final states. Then, the four decay channels are $(N\pi)_{S,I=1/2}$, $(N\pi)_{S,I=3/2}$, $(N\pi)_{P,I=1/2}$, and $(N\pi)_{P,I=3/2}$. Following the conventions of the main text, we denote the corresponding decay amplitudes by $L_{1,1}$ for $I = 1/2$ and by $L_{3,3}$ for $I = 3/2$; here, $L = S, P$. The initial decay amplitudes that emerge from the weak process are denoted by $L^{\rm ini}_{\ldots}$. For the corresponding antiparticle decays, we use $\bar{L}_{\ldots}$. We assume baryon number conservation. Then, there are no oscillations between Λ and its antiparticle $\bar{\Lambda}$. But the final-state interactions (FSIs) might allow for transitions between the four final states $(N\pi)_{S,I=1/2}$, $(N\pi)_{S,I=3/2}$, $(N\pi)_{P,I=1/2}$, and $(N\pi)_{P,I=3/2}$. This defines a coupled-channel problem. We assume that the weak process is of short-distance nature such that no structure is resolved. Therefore, the discontinuity of a decay amplitude is solely given by the FSIs. This defines an Omnès problem [95]; for an analogous situation, see, e.g., Ref. [94].

In general, one has a 4×4 Omnès-function matrix Ω that parametrizes the FSI. This matrix maps the "bare" amplitudes of the initial decay onto the "full" amplitudes that contain the FSI:

$$\begin{pmatrix} S_{1,1} \\ S_{3,3} \\ P_{1,1} \\ P_{3,3} \end{pmatrix} = \Omega \begin{pmatrix} S^{\rm ini}_{1,1} \\ S^{\rm ini}_{3,3} \\ P^{\rm ini}_{1,1} \\ P^{\rm ini}_{3,3} \end{pmatrix}. \tag{C1}$$

The corresponding equation for the antiparticle sector reads

$$\begin{pmatrix} \bar{S}_{1,1} \\ \bar{S}_{3,3} \\ \bar{P}_{1,1} \\ \bar{P}_{3,3} \end{pmatrix} = \bar{\Omega} \begin{pmatrix} \bar{S}^{\rm ini}_{1,1} \\ \bar{S}^{\rm ini}_{3,3} \\ \bar{P}^{\rm ini}_{1,1} \\ \bar{P}^{\rm ini}_{3,3} \end{pmatrix}. \tag{C2}$$

Next, we assume that parity and charge conjugation are both conserved by the FSI. This is true for strong and electromagnetic FSI. In this case, the FSIs are the same in the particle and antiparticle sector, i.e., $\Omega = \bar{\Omega}$, and there is no cross-talk between the parity-even p waves and the parity-odd s waves:

$$\Omega = \bar{\Omega} = \begin{pmatrix} \Omega_S & 0 \\ 0 & \Omega_P \end{pmatrix} \tag{C3}$$

with 2×2 matrices Ω_S and Ω_P.

Finally, we assume isospin symmetry. Then, the 2×2 matrices become diagonal. Watson's theorem [66] ensures that the phase of the pertinent Omnès function agrees with the scattering phase shift $\delta_{L,2I}$ of the corresponding $N - \pi$ scattering:

$$\Omega_L = {\rm diag}(|\Omega_{L,2I=1}|e^{i\delta_{L,1}}, |\Omega_{L,2I=3}|e^{i\delta_{L,3}}) \tag{C4}$$

with $L = S$, P. Here, it is of advantage that we changed from the particle basis ($p\pi^-$ and $n\pi^0$) to the isospin basis ($I = 1/2$ and $I = 3/2$). In the particle basis, the 2×2 Omnès matrices would not be diagonal.

Of course, if required by precision, the assumptions that lead from more general 4×4 matrices in (C1) and (C2) to (C3) and (C4) can be relaxed one by one.

APPENDIX D: AVERAGE POLARIZATION AND SPIN-CORRELATION TERMS

Expression for average polarization squared

$$\langle \mathbf{P}_B^2 \rangle = \int \mathbf{P}_B^2 \left(\frac{1}{\sigma} \frac{\mathrm{d}\sigma}{\mathrm{d}\Omega_B} \right) \mathrm{d}\Omega_B = \frac{3}{2} \int \mathbf{P}_B^2 \frac{1 + \alpha_\psi \cos^2\theta}{3 + \alpha_\psi} \mathrm{d}\cos\theta, \tag{D1}$$

where $\mathbf{P}_B$ is given by Eq. (40). The integral can be calculated exactly, and the result is expressed as

$$\langle \mathbf{P}_B^2 \rangle = \mathbb{p}_0 + \mathbb{p}_2 P_e^2, \tag{D2}$$

where

$$\mathbb{p}_0 = \frac{(1 - \alpha_\psi^2)\sin^2(\Delta\Phi)}{\alpha_\psi^2(3 + \alpha_\psi)} \{3 + 2\alpha_\psi - 3(1 + \alpha_\psi)\mathrm{F}(\alpha_\psi)\}, \tag{D3}$$

$$\mathbb{p}_2 = \frac{3(1 + \alpha_\psi)^2}{\alpha_\psi(3 + \alpha_\psi)} \left\{ 1 - \frac{1 - \alpha_\psi}{1 + \alpha_\psi} \cos^2(\Delta\Phi) - (1 - (1 - \alpha_\psi)\cos^2(\Delta\Phi))\mathrm{F}(\alpha_\psi) \right\}. \tag{D4}$$

The function $F(\alpha)$ is

$$F(\alpha) \coloneqq \int_0^1 \frac{\mathrm{d}x}{1 + \alpha x^2} = \begin{cases} \frac{\arctan\sqrt{\alpha}}{\sqrt{\alpha}} & 0 < \alpha \leq 1 \\ 1 & \alpha = 0 \\ \frac{\operatorname{arctanh}\sqrt{|\alpha|}}{\sqrt{|\alpha|}} & -1 < \alpha < 0 \end{cases}. \tag{D5}$$

Properties of the function $F(1) = \frac{\pi}{4}$ and $\lim_{\alpha \to -1} F(\alpha) = \infty$. The function is drawn in Fig. 18. For $\alpha_\psi = 1$, the coefficients are

$$\mathbb{p}_0 = 0 \quad \text{and} \quad \mathbb{p}_2 = \frac{3(4 - \pi)}{4} \approx 0.6438, \tag{D6}$$

and for $\alpha_\psi = 0$,

$$\mathbb{p}_0 = \frac{2}{15}\sin^2(\Delta\Phi) \quad \text{and} \quad \mathbb{p}_2 = \frac{2 + \cos(2\Delta\Phi)}{3}. \tag{D7}$$

One derives similar expressions for the sum of the squares of the spin-correlation terms. The result can be expressed as

$$\langle \mathbb{S}_{B\bar{B}}^2 \rangle = \mathbb{s}_0 + \mathbb{s}_2 P_e^2, \tag{D8}$$

where

$$\begin{aligned} \mathbb{s}_0 = \frac{1}{\alpha_\psi^2(3 + \alpha_\psi)} \{ & (1 - \alpha_\psi^2)(2\alpha_\psi + 3)\cos(2\Delta\Phi) - 7\alpha_\psi^3 - 2\alpha_\psi - 3 \\ & - 3(\alpha_\psi + 1)^2 F(\alpha_\psi)[(1 - \alpha_\psi)\cos(2\Delta\Phi) + \alpha_\psi - 2\alpha_\psi^2 - 1]\}, \end{aligned} \tag{D9}$$

$$\mathbb{s}_2 = \frac{6(1 - \alpha_\psi^2)\sin^2(\Delta\Phi)}{\alpha_\psi(3 + \alpha_\psi)} \{(1 + \alpha_\psi)F(\alpha_\psi) - 1\}. \tag{D10}$$

For the $e^+e^- \to B\bar{B}$ process specified by the parameters α_ψ, β_ψ, and γ_ψ, the polarization and spin-correlation terms as a function of the B-baryon production angle θ are

$$\mathbb{P}_B^2(\cos\theta) = 2\frac{(\alpha_\psi + 1)^2 P_e^2 \cos^2\theta + \sin^2\theta(\beta_\psi^2 \cos^2\theta + P_e^2\gamma_\psi^2)}{(1 + \alpha_\psi \cos^2\theta)^2}, \tag{D11}$$

$$\mathbb{S}_{B\bar{B}}^2(\cos\theta) = \frac{(\alpha_\psi^2 + 1)\sin^4\theta + (\alpha_\psi + \cos^2\theta)^2 + 2\sin^2\theta(\gamma_\psi^2 \cos^2\theta + P_e^2\beta_\psi^2)}{(1 + \alpha_\psi \cos^2\theta)^2}. \tag{D12}$$

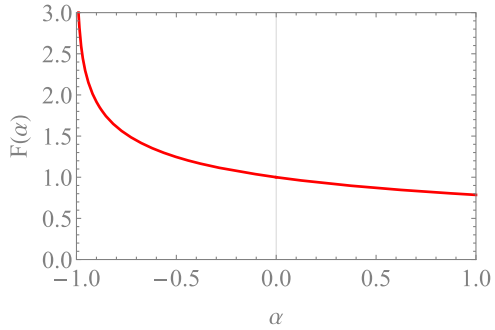

FIG. 18. Function $F(\alpha)$ defined in Eq. (D5). The function is divergent for $\alpha \to -1$.

APPENDIX E: MODIFICATION OF THE FISHER INFORMATION MATRICES TO INCLUDE BACKGROUND

Neglecting the resolution effect for the $\boldsymbol{\xi}$ variables, the overall probability density function including background term, $\mathcal{P}^B(\boldsymbol{\xi})$, and relative detection efficiency, $\epsilon(\boldsymbol{\xi})$, is

$$\mathcal{P}^T(\boldsymbol{\xi};\boldsymbol{\omega}) = p\mathcal{P}(\boldsymbol{\xi};\boldsymbol{\omega})\epsilon(\boldsymbol{\xi}) + (1-p)\mathcal{P}^B(\boldsymbol{\xi}). \quad \text{(E1)}$$

We impose the normalization $\int \mathcal{P}^B(\boldsymbol{\xi})\mathrm{d}\boldsymbol{\xi} = 1$ for the background and $\int \mathcal{P}(\boldsymbol{\xi};\boldsymbol{\omega})\epsilon(\boldsymbol{\xi})\mathrm{d}\boldsymbol{\xi} = 1$ for the signal. The last condition implies that the relative efficiency $\epsilon(\boldsymbol{\xi})$ must be equal to one if it is constant. The coefficient $p = S/N$ represents the ratio of the number of the signal events, S, to the total number of the signal and background events N. It is assumed that the ratio is fixed and has a known value. The Fisher information matrix Eq. (52) now reads

$$\begin{aligned}\mathcal{I}(\omega_k,\omega_l) &:= N\int \frac{1}{\mathcal{P}^T}\frac{\partial\mathcal{P}^T}{\partial\omega_k}\frac{\partial\mathcal{P}^T}{\partial\omega_l}\mathrm{d}\boldsymbol{\xi} \\ &= Np^2\int \frac{1}{\mathcal{P}^T}\frac{\partial\mathcal{P}}{\partial\omega_k}\frac{\partial\mathcal{P}}{\partial\omega_l}\epsilon^2(\boldsymbol{\xi})\mathrm{d}\boldsymbol{\xi}. \end{aligned} \quad \text{(E2)}$$

We rewrite the background distribution as

$$\mathcal{P}^B(\boldsymbol{\xi}) =: \frac{1+\mathcal{G}^B(\boldsymbol{\xi})}{\mathcal{V}} \quad \text{(E3)}$$

and use Eq. (57) representation for the signal with $C_{00} = 1$. The term $1/\mathcal{P}^T$ can be therefore written as

$$\frac{1}{\mathcal{P}^T} = \frac{\mathcal{V}}{1+p(\epsilon-1)+p\mathcal{G}\epsilon+(1-p)\mathcal{G}^B} \quad \text{(E4)}$$

$$\approx \frac{\mathcal{V}}{1+p\mathcal{G}}, \quad \text{(E5)}$$

where the approximate form is obtained by setting $\epsilon(\boldsymbol{\xi}) = \text{const.} \equiv 1$ and $\mathcal{G}^B = 0$. Therefore, the analytical 0th order approximations for experiments with background can be obtained by replacing $N \to S^2/N$ in our expressions.

[1] A. D. Sakharov, Pis'ma Zh. Eksp. Teor. Fiz. **5**, 32 (1967) [Usp. Fiz. Nauk **161**, 61 (1991)].
[2] V. A. Kuzmin, V. A. Rubakov, and M. E. Shaposhnikov, Phys. Lett. **155B**, 36 (1985).
[3] M. E. Shaposhnikov, Phys. Lett. B **277**, 324 (1992); **282**, 483(E) (1992).
[4] J. H. Christenson, J. W. Cronin, V. L. Fitch, and R. Turlay, Phys. Rev. Lett. **13**, 138 (1964).
[5] B. Aubert *et al.* (*BABAR* Collaboration), Phys. Rev. Lett. **87**, 091801 (2001).
[6] K. Abe *et al.* (Belle Collaboration), Phys. Rev. Lett. **87**, 091802 (2001).
[7] A. J. Buras, R. Fleischer, S. Recksiegel, and F. Schwab, Eur. Phys. J. C **32**, 45 (2003).
[8] R. Aaij *et al.* (LHCb Collaboration), Phys. Rev. Lett. **122**, 211803 (2019).
[9] J. R. Batley *et al.* (NA48 Collaboration), Phys. Lett. B **544**, 97 (2002).
[10] A. Alavi-Harati *et al.* (KTeV Collaboration), Phys. Rev. D **67**, 012005 (2003); **70**, 079904(E) (2004).
[11] E. Abouzaid *et al.* (KTeV Collaboration), Phys. Rev. D **83**, 092001 (2011).
[12] A. Buras, Acta Phys. Pol. B **52**, 7 (2021).
[13] Z. Bai *et al.* (RBC, UKQCD Collaborations), Phys. Rev. Lett. **115**, 212001 (2015).
[14] R. Abbott *et al.* (RBC, UKQCD Collaborations), Phys. Rev. D **102**, 054509 (2020).
[15] H. Gisbert and A. Pich, Rep. Prog. Phys. **81**, 076201 (2018).
[16] J. Aebischer, C. Bobeth, and A. J. Buras, Eur. Phys. J. C **80**, 705 (2020).
[17] S. Okubo, Phys. Rev. **109**, 984 (1958).
[18] A. Pais, Phys. Rev. Lett. **3**, 242 (1959).
[19] T. Brown, S. F. Tuan, and S. Pakvasa, Phys. Rev. Lett. **51**, 1823 (1983).
[20] L.-L. Chau and H.-Y. Cheng, Phys. Lett. **131B**, 202 (1983).
[21] J. F. Donoghue and S. Pakvasa, Phys. Rev. Lett. **55**, 162 (1985).
[22] J. F. Donoghue, X.-G. He, and S. Pakvasa, Phys. Rev. D **34**, 833 (1986).
[23] T. D. Lee and C.-N. Yang, Phys. Rev. **108**, 1645 (1957).
[24] P. M. Ho *et al.*, Phys. Rev. D **44**, 3402 (1991).
[25] R. A. Burnstein *et al.* (HyperCP Collaboration), Nucl. Instrum. Methods Phys. Res., Sect. A **541**, 516 (2005).

[26] J. Tandean and G. Valencia, Phys. Rev. D **67**, 056001 (2003).
[27] T. Holmstrom *et al.* (HyperCP Collaboration), Phys. Rev. Lett. **93**, 262001 (2004).
[28] P. A. Zyla *et al.* (Particle Data Group), Prog. Theor. Exp. Phys. **2020**, 083C01 (2020).
[29] N. Cabibbo and R. Gatto, Phys. Rev. **124**, 1577 (1961).
[30] A. Z. Dubnickova, S. Dubnicka, and M. P. Rekalo, Nuovo Cimento A **109**, 241 (1996).
[31] M. Ablikim *et al.* (BESIII Collaboration), Nat. Phys. **15**, 631 (2019).
[32] M. Ablikim *et al.* (BESIII Collaboration), Nature (London) **606**, 64 (2022).
[33] C.-Z. Yuan and S. L. Olsen, Nat. Rev. Phys. **1**, 480 (2019).
[34] Q. Luo and D. R. Xu, Progress on preliminary conceptual study of HIEPA, a super Tau-Charm factory in China, in *Proceedings of the 9th International Particle Accelerator Conference*, International Particle Accelerator Conference (JACoW Publishing, Geneva, Switzerland, 2018), pp. 422–424, 10.18429/JACoW-IPAC2018-MOPML013.
[35] E. B. Levichev, A. N. Skrinsky, G. M. Tumaikin, and Y. M. Shatunov, Phys. Usp. **61**, 405 (2018).
[36] M.-H. Ye and Z.-P. Zheng, Int. J. Mod. Phys. A **02**, 1707 (1987).
[37] M. Ablikim *et al.* (BESIII Collaboration), Nucl. Instrum. Methods Phys. Res., Sect. A **614**, 345 (2010).
[38] A. Renieri, Possibility of achieving very high-energy resolution in electron-positron storage rings, Report No. lNF-75/6-R, 1975.
[39] A. A. Avdienko, G. A. Kornyukhin, I. Y. Protopopov, A. N. Skrinsky, A. B. Temnykh, G. M. Tumaikin, and A. A. Zholents, Conf. Proc. C **830811**, 186 (1983).
[40] V. I. Telnov, arXiv:2008.13668.
[41] I. Koop, A. Bogomyagkov, and A. Otboev, in *Joint Workshop on Future charm-tau Factory* (Russian Academy of Sciences, Moscow, 2019), https://c-tau.ru/indico/event/3/contributions/206/.
[42] A. Kupsc, in *Joint Workshop on Future charm-tau Factory* (Russian Academy of Sciences, Moscow, 2019), https://c-tau.ru/indico/event/3/contributions/171/.
[43] A. Bondar, A. Grabovsky, A. Reznichenko, A. Rudenko, and V. Vorobyev, J. High Energy Phys. 03 (2020) 076.
[44] M. Jacob and G. C. Wick, Ann. Phys. (N.Y.) **7**, 404 (1959); **281**, 774 (2000).
[45] E. Perotti, G. Fäldt, A. Kupsc, S. Leupold, and J. J. Song, Phys. Rev. D **99**, 056008 (2019).
[46] P. Adlarson and A. Kupsc, Phys. Rev. D **100**, 114005 (2019).
[47] D. G. Ireland, M. Döring, D. I. Glazier, J. Haidenbauer, M. Mai, R. Murray-Smith, and D. Rönchen, Phys. Rev. Lett. **123**, 182301 (2019).
[48] R. Handler *et al.*, Phys. Rev. D **25**, 639 (1982).
[49] J. R. Batley *et al.* (NA48 Collaboration), Phys. Lett. B **693**, 241 (2010).
[50] M. Huang *et al.* (HyperCP Collaboration), Phys. Rev. Lett. **93**, 011802 (2004).
[51] W. E. Cleland, G. Conforto, G. H. Eaton, H. J. Gerber, M. Reinharz, A. Gautschi, E. Heer, C. Revillard, and G. Von Dardel, Nucl. Phys. **B40**, 221 (1972).
[52] O. E. Overseth and R. F. Roth, Phys. Rev. Lett. **19**, 391 (1967).
[53] J. W. Cronin and O. E. Overseth, Phys. Rev. **129**, 1795 (1963).
[54] M. Ablikim *et al.* (BESIII Collaboration), Phys. Rev. Lett. **125**, 052004 (2020).
[55] F. Harris, O. E. Overseth, L. Pondrom, and E. Dettmann, Phys. Rev. Lett. **24**, 165 (1970).
[56] N. H. Lipman *et al.*, Phys. Lett. **43B**, 89 (1973).
[57] V. Cirigliano, G. Ecker, H. Neufeld, and A. Pich, Eur. Phys. J. C **33**, 369 (2004).
[58] M. Hoferichter, J. Ruiz de Elvira, B. Kubis, and U.-G. Meißner, Phys. Rep. **625**, 1 (2016).
[59] R. Nath and A. Kumar, Nuovo Cimento **36**, 669 (1965).
[60] M. Lu, M. B. Wise, and M. J. Savage, Phys. Lett. B **337**, 133 (1994).
[61] A. N. Kamal, Phys. Rev. D **58**, 077501 (1998).
[62] A. Datta, P. O'Donnell, and S. Pakvasa, Λ—π phase shifts in chiral perturbation theory, Report No. UTPT-98-09, UH-511-852-98, FERMILAB-PUB-98-185-T (1998), arXiv:hep-ph/9806374.
[63] J. Tandean, A. W. Thomas, and G. E. Valencia, Phys. Rev. D **64**, 014005 (2001).
[64] U.-G. Meissner and J. A. Oller, Phys. Rev. D **64**, 014006 (2001).
[65] B.-L. Huang, J.-S. Zhang, Y.-D. Li, and N. Kaiser, Phys. Rev. D **96**, 016021 (2017).
[66] K. M. Watson, Phys. Rev. **95**, 228 (1954).
[67] J. Tandean, Phys. Rev. D **69**, 076008 (2004).
[68] D. Chang, X.-G. He, and S. Pakvasa, Phys. Rev. Lett. **74**, 3927 (1995).
[69] X.-G. He and G. Valencia, Phys. Rev. D **52**, 5257 (1995).
[70] A. J. Buras, G. Colangelo, G. Isidori, A. Romanino, and L. Silvestrini, Nucl. Phys. **B566**, 3 (2000).
[71] X.-G. He, H. Murayama, S. Pakvasa, and G. Valencia, Phys. Rev. D **61**, 071701 (2000).
[72] C.-H. Chen, Phys. Lett. B **521**, 315 (2001).
[73] V. Cirigliano, H. Gisbert, A. Pich, and A. Rodríguez-Sánchez, J. High Energy Phys. 02 (2020) 032.
[74] J. Brod, M. Gorbahn, and E. Stamou, Phys. Rev. Lett. **125**, 171803 (2020).
[75] J. Aebischer, A. J. Buras, and J. Kumar, J. High Energy Phys. 12 (2020) 097.
[76] S. R. Beane, P. F. Bedaque, A. Parreno, and M. J. Savage, Nucl. Phys. **A747**, 55 (2005).
[77] C. G. White *et al.*, Nucl. Phys. B, Proc. Suppl. **71**, 451 (1999).
[78] C. Materniak (HyperCP Collaboration), Nucl. Phys. B, Proc. Suppl. **187**, 208 (2009).
[79] G. Fäldt and A. Kupść, Phys. Lett. B **772**, 16 (2017).
[80] M. Ablikim *et al.* (BESIII Collaboration), Phys. Rev. D **95**, 052003 (2017).
[81] M. Ablikim *et al.* (BES Collaboration), Phys. Rev. D **78**, 092005 (2008).
[82] M. Ablikim *et al.* (BESIII Collaboration), Phys. Lett. B **770**, 217 (2017).
[83] S. J. Brodsky and G. P. Lepage, Phys. Rev. D **24**, 2848 (1981).
[84] R. A. Fisher and E. J. Russell, Phil. Trans. R. Soc. A **222**, 309 (1922).
[85] I. I. Bigi, X.-W. Kang, and H.-B. Li, Chin. Phys. C **42**, 013101 (2018).

[86] M. Ablikim *et al.* (BESIII Collaboration), Phys. Rev. D **93**, 072003 (2016).
[87] Y. B. Li *et al.* (Belle Collaboration), Phys. Rev. Lett. **127**, 121803 (2021).
[88] O. E. Overseth and S. Pakvasa, Phys. Rev. **184**, 1663 (1969).
[89] M. Suzuki, Phys. Rev. D **66**, 054018 (2002).
[90] J. P. Dedonder, A. Furman, R. Kaminski, L. Lesniak, and B. Loiseau, Acta Phys. Pol. B **42**, 2013 (2011).
[91] D.-L. Yao, L.-Y. Dai, H.-Q. Zheng, and Z.-Y. Zhou, Rep. Prog. Phys. **84**, 076201 (2021).
[92] L.-Y. Dai and M. R. Pennington, Phys. Rev. D **90**, 036004 (2014).
[93] Y.-J. Shi, U.-G. Meißner, and Z.-X. Zhao, Eur. Phys. J. C **82**, 113 (2022).
[94] J. T. Daub, C. Hanhart, and B. Kubis, J. High Energy Phys. 02 (2016) 009.
[95] R. Omnes, Nuovo Cimento **8**, 316 (1958).